REPORT DOCUMENTATION PAGE

Form Approved OMB NO. 0704-0188

1. REPORT DATE (DD-MM-YYYY)	2. REPORT TYPE	3. DATES COVERED (From - To)
24-08-2015	Ph.D. Dissertation	-

4. TITLE AND SUBTITLE
Enhancing Aluminum Reactivity by Exploiting Surface Chemistry and Mechanical Properties

5a. CONTRACT NUMBER
W911NF-14-1-0250

5b. GRANT NUMBER

5c. PROGRAM ELEMENT NUMBER
611102

6. AUTHORS
Jena McCollum

5d. PROJECT NUMBER

5e. TASK NUMBER

5f. WORK UNIT NUMBER

7. PERFORMING ORGANIZATION NAMES AND ADDRESSES
Texas Technical University
Box 41035
349 Admin Bldg
Lubbock, TX 79409 -1035

8. PERFORMING ORGANIZATION REPORT NUMBER

9. SPONSORING/MONITORING AGENCY NAME(S) AND ADDRESS (ES)
U.S. Army Research Office
P.O. Box 12211
Research Triangle Park, NC 27709-2211

10. SPONSOR/MONITOR'S ACRONYM(S)
ARO

11. SPONSOR/MONITOR'S REPORT NUMBER(S)
64880-EG.11

12. DISTRIBUTION AVAILIBILITY STATEMENT
Approved for public release; distribution is unlimited.

13. SUPPLEMENTARY NOTES
The views, opinions and/or findings contained in this report are those of the author(s) and should not contrued as an official Department of the Army position, policy or decision, unless so designated by other documentation.

14. ABSTRACT
Metal-fluoropolymer based systems have drawn quite a bit of attention in the combustion community in recent years due to the exothermic surface chemistry between fluorine (F) and the alumina (Al2O3) shell surrounding aluminum (Al) fuel particles promotes aluminum reactivity. Incorporating a liquid fluorinated oligomer, specifically perfluoropolyether (PFPE), exhibits this surface chemistry while increasing the proximity of fuel and oxidizer.
Flame speeds, differential scanning calorimetry (DSC), thermogravimetric analysis (TGA) and quadruple mass

15. SUBJECT TERMS
aluminum combustion, reaction kinetics, exothermic surface chemistry, fluorine, aluminum fluoride, energy propagation

16. SECURITY CLASSIFICATION OF:			17. LIMITATION OF ABSTRACT	15. NUMBER OF PAGES	19a. NAME OF RESPONSIBLE PERSON
a. REPORT	b. ABSTRACT	c. THIS PAGE			Michelle Pantoya
UU	UU	UU	UU		19b. TELEPHONE NUMBER 806-742-3563

Report Title

Enhancing Aluminum Reactivity by Exploiting Surface Chemistry and Mechanical Properties

ABSTRACT

Metal-fluoropolymer based systems have drawn quite a bit of attention in the combustion community in recent years due to the exothermic surface chemistry between fluorine (F) and the alumina (Al2O3) shell surrounding aluminum (Al) fuel particles promotes aluminum reactivity. Incorporating a liquid fluorinated oligomer, specifically perfluoropolyether (PFPE), exhibits this surface chemistry while increasing the proximity of fuel and oxidizer. Flame speeds, differential scanning calorimetry (DSC), thermogravimetric analysis (TGA) and quadruple mass spectrometry (QMS) were performed for a variety of Al particle sizes blended with PFPE. The results show that the combustion performance of these blends is highly dependent on the Al2O3 concentration and exposed surface area. As Al particle diameter increases from 80 to 120 nm, the Al-PFPE blends exhibit an increase in flame speeds by 48%, but from 120 to 5500 nm, flame speeds decrease by 93%. There is a balance to optimizing Al particle reactivity with PFPE coating between activating Al particles with exothermic surface chemistry versus the unreacted alumina that contributes a thermal heat sink during energy generation.

Many Al fueled energetic composites use solid oxidizers that induce no alumina surface exothermicity, such as molybdenum trioxide (MoO3) or copper oxide (CuO). To further understand the role of PFPE in energetic systems, varying concentrations were blended with Al/CuO and Al/MoO3 thermites. Flame speeds, differential scanning calorimetry (DSC) and quadruple mass spectrometry (QMS) were performed for varying percent PFPE blended with Al/MoO3 or Al/CuO in order to examine reaction kinetics and combustion performance. X-ray photoelectron spectroscopy (XPS) was performed to identify product species. Results show that the performance of the thermite-PFPE blends is highly dependent on the bond dissociation energy of the metal oxide. Fluorine-aluminum based surface exothermic chemistry with MoO3 produce an increase in reactivity while the blends with CuO show a decline when increasing the PFPE loadings. These results provide new evidence that optimizing aluminum combustion can be achieved through activating exothermic Al surface chemistry that produces aluminum fluoride.

Another avenue for increasing Al reactivity is to alter its mechanical properties. In bulk material processing, annealing and quenching metals such as Al can relieve residual stress and improve mechanical properties. On a single particle level, affecting mechanical properties may also affect Al particle reactivity. Aluminum particles underwent thermal treatment in order to examine the effect of annealing and quenching on the strain of Al particles and the corresponding reactivity of Al and CuO composites. Synchrotron X-ray diffraction (XRD) analysis of the particles reveals the thermal treatment increased the dilatational strain of the aluminum-core, alumina-shell particles. Flame propagation experiments also show thermal treatments effect reactivity when combined with CuO. An effective annealing/quenching treatment for increasing aluminum reactivity was identified. These results show that altering the mechanical properties of Al particles affects their reactivity.

Enhancing Aluminum Reactivity by Exploiting Surface Chemistry and Mechanical Properties

by

Jena McCollum, B.S.M.E.

A Dissertation In

MECHANICAL ENGINEERING

Submitted to the Graduate Faculty

of Texas Tech University in

Partial Fulfillment of the Requirements for

the Degree of

DOCTOR OF PHILOSOPHY

Michelle Pantoya
Chair of Committee

Jharna Chaudhuri

Gordon Christopher

Stephen Ekwaro-Osire

Luciano Castillo

June, 2015

ACKNOWLEDGEMENTS

When I made the decision to move to Lubbock to pursue graduate school, I had no idea what to expect. My husband and I, with two babies in tow, made the journey and arrived to the beginning of an intimidating goal. There were times when balancing research, classes, motherhood and a marriage seemed like an impossible task, but thanks to the guidance and patience of those I have had the pleasure to know in the last few years, I find myself finally writing this dissertation.

First, I want to thank my mentor, Dr. Michelle Pantoya. It has been incredibly humbling to work for you. At times, when I would wonder how any human could manage to excel in both engineering and motherhood, I had you to look to. I have such incredible respect for you in whatever hat (or hats) you may wear each day.

I would also like to thank Dr. Emily Hunt. You inspired me to even attempt graduate school. I'm so grateful that you took the time and interest to help me get here. You are an inspiration and I am so lucky to know you. To my lab mates, Billy: thank you for challenging me and keeping me thinking. Cory: thank you for your kindness, invaluable guidance and patience as I had a million questions for

you every day. Keerti: you taught me so much. You've not only been an incredible mentor, but an incredible friend.

Next, I want to thank my mom and dad. I know that graduate school seemed like a terrifying option a few years ago, but you never stopped telling me how proud you were and that has made all of the difference. Thank you for being there to catch us more than a few times. I only hope that I am able to take care of you the way you have cared for me and my family. I love you guys so much.

To my beautiful children, Malachi and Avery: you are the reason for all of this. You are the reason that I keep pushing to be better. I would crawl to the ends of the earth for you. My primary goal is to show you that no matter what happens in life, no matter what cards you are dealt, that you are the deciding factor in your own outcome. Never let anyone tell you that you can't have what you want. Never stop learning. Never stop trying. Never stop growing. Momma loves you more than you could understand.

Finally, I want to thank my amazing husband, Patrick. The end of this road has finally arrived. We've both grown and seen so much in the last 8 years and you've spent that time helping me down this road, carrying me for some of it.

Words cannot express how precious you are to me. I will spend the rest of my life trying to repay you for helping me reach my dream. I love you so much.

Additionally, I would like to acknowledge the Army Research Office for supporting my research via a grant (W911-NF-14-1-0250). I am sincerely appreciative of this support!

Table of Contents

ABSTRACT

Metal-fluoropolymer based systems have drawn quite a bit of attention in the combustion community in recent years due to the exothermic surface chemistry between fluorine (F) and the alumina (Al_2O_3) shell surrounding aluminum (Al) fuel particles promotes aluminum reactivity. Incorporating a liquid fluorinated oligomer, specifically perfluoropolyether (PFPE), exhibits this surface chemistry while increasing the proximity of fuel and oxidizer.

Flame speeds, differential scanning calorimetry (DSC), thermogravimetric analysis (TGA) and quadruple mass spectrometry (QMS) were performed for a variety of Al particle sizes blended with PFPE. The results show that the combustion performance of these blends is highly dependent on the Al_2O_3 concentration and exposed surface area. As Al particle diameter increases from 80 to 120 nm, the Al-PFPE blends exhibit an increase in flame speeds by 48%, but from 120 to 5500 nm, flame speeds decrease by 93%. There is a balance to optimizing Al particle reactivity with PFPE coating between activating Al particles with exothermic surface chemistry versus the unreacted alumina that contributes a thermal heat sink during energy generation.

Many Al fueled energetic composites use solid oxidizers that induce no alumina surface exothermicity, such as molybdenum trioxide (MoO_3) or copper

oxide (CuO). To further understand the role of PFPE in energetic systems, varying concentrations were blended with Al/CuO and Al/MoO_3 thermites. Flame speeds, differential scanning calorimetry (DSC) and quadruple mass spectrometry (QMS) were performed for varying percent PFPE blended with Al/MoO_3 or Al/CuO in order to examine reaction kinetics and combustion performance. X-ray photoelectron spectroscopy (XPS) was performed to identify product species. Results show that the performance of the thermite-PFPE blends is highly dependent on the bond dissociation energy of the metal oxide. Fluorine-aluminum based surface exothermic chemistry with MoO_3 produce an increase in reactivity while the blends with CuO show a decline when increasing the PFPE loadings. These results provide new evidence that optimizing aluminum combustion can be achieved through activating exothermic Al surface chemistry that produces aluminum fluoride.

Another avenue for increasing Al reactivity is to alter its mechanical properties. In bulk material processing, annealing and quenching metals such as Al can relieve residual stress and improve mechanical properties. On a single particle level, affecting mechanical properties may also affect Al particle reactivity. Aluminum particles underwent thermal treatment in order to examine the effect of annealing and quenching on the strain of Al particles and the

corresponding reactivity of Al and CuO composites. Synchrotron X-ray diffraction (XRD) analysis of the particles reveals the thermal treatment increased the dilatational strain of the aluminum-core, alumina-shell particles. Flame propagation experiments also show thermal treatments effect reactivity when combined with CuO. An effective annealing/quenching treatment for increasing aluminum reactivity was identified. These results show that altering the mechanical properties of Al particles affects their reactivity.

List of Figures

List of Tables

CHAPTER I: Fundamentals of Combustion

From early times, combustion has been observed and studied by curious minds. One of the earliest concepts was the phlogiston theory which was conceptualized by Johann Joachim Becher in the 17th century. This basically stated that all substances were comprised of three kinds of earth; the vitrifiable, the mercurial, and the combustible.

Combustion can be studied in gas (i.e., natural gas), liquid (i.e., gasoline, kerosene) and solid (i.e., coal, thermites, etc.) phases. Although the reaction mechanisms vary among the different phases, basic combustion characteristics can be calculated for any combustible medium.

Activation Energy and Heat of Combustion

Combustion reactions occur by exothermic reactions. This occurs when the energy of the products is lower than the energy of the reactants. This means that heat was released from the system. Figure 1 shows how the energy changes in these systems during the reaction.

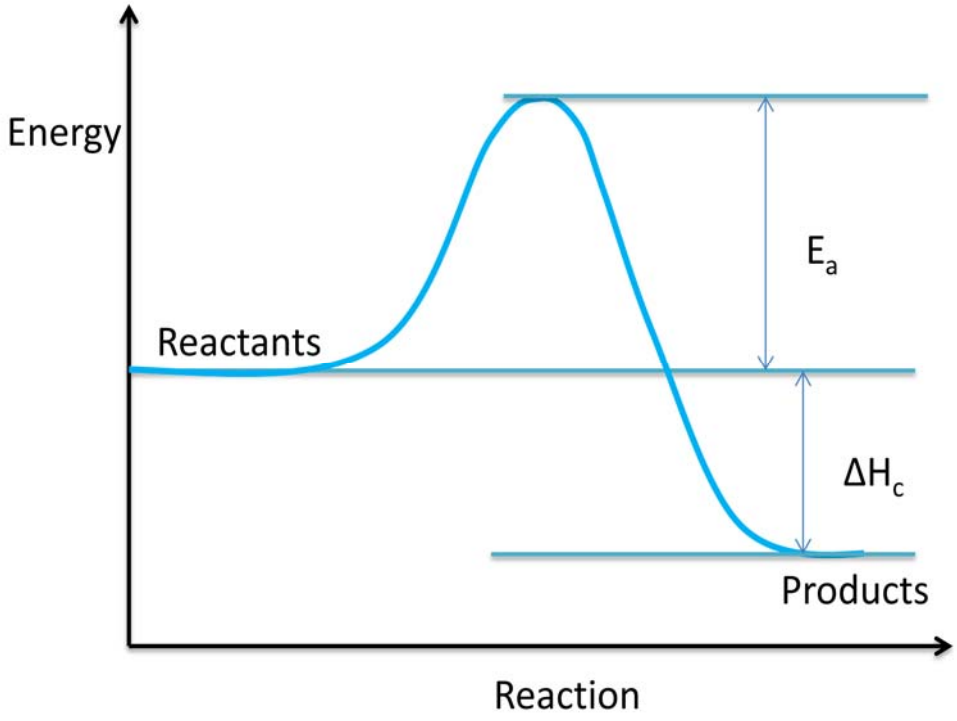

Figure 1. Energy change of an exothermic reaction

In order to have a reaction, the energy level of the reactants must be raised from their equilibrium state to the minimum energy for the reaction to occur. The minimum energy needed to start a reaction is called the activation energy (E_a). The activation energy is related to the reaction rate (k(t)) and shown in Eq. (1) where *A* is the pre-exponential factor, *R* is the universal gas constant and *T* is the temperature.

$$\mathbf{k(t) = Aexp(-\frac{E_a}{RT})} \qquad (1)$$

The heat of combustion *(ΔH_c)* is given by Hess' Law shown in Eq. (2).

$$\Delta \mathbf{H_c} = \sum_{\mathbf{react}} \mathbf{H_f^o} - \sum_{\mathbf{prod}} \mathbf{H_f^o} \qquad (2)$$

This means that the ΔH_c is the difference in the heat of formation of the reactants and the heat of formation of the products. This translates to the amount of heat liberated from the reaction. The necessary information about reactants (fuel and oxidizer) and the products can be obtained in the reaction equation.

Reaction Equations

Combustion takes place by an oxidative reaction. The reactant that is reduced in the reaction is called the fuel. In gas and liquid combustion, these fuels are typically hydrocarbons. Their reduction by air or pure oxygen results in water (H_2O), carbon dioxide (CO_2), and other intermediates (CO, OH, C, O_2, N_2, etc.). In simplified combustion, these intermediates may not be present in the reaction formula. For example, the reaction equation for general hydrocarbon (C_xH_y) combustion with oxygen (O_2) is shown in Eq. (3).

$$aC_xH_y + bO_2 \rightarrow cCO_2 + dH_2O \qquad (3)$$

This equation assumes no production of intermediates (i.e. CO, OH, etc). The coefficients *a*, *b*, *c*, and *d* can be deduced by performing a molar balance of all elements. Because this reaction is considered for only 1 mole of C_xH_y, and C_xH_y has *ax* carbon (C) atoms, *c* must equal *ax*. Next, the hydrogen (H) atoms will be balanced. The hydrocarbon has *ay* H atoms, which means that *d* must equal

ay/2. Now that *c* and *d* have been obtained, *b* can be found. With *c*=*ax* and *d*=*ay/2*, the products contain a total of *2a(x+y/4)* O atoms. This means that *b* must equal *a(x+y/4)*. The final equation is shown in Eq. (4).

$$aC_xH_y + a(x+y/4)O_2 \rightarrow axCO_2 + a(y/2)H_2O \qquad (4)$$

Stoichiometry

An important factor in combustion is the relationship between fuel and oxidizer in the reaction. If the reaction is fuel rich, there will be remaining fuel in the products. If the reaction is fuel lean, the products will contain unused oxidizer (i.e., O_2, N_2, etc). This characteristic is known as an equivalence ratio (ER). For

ER=1, the mixture is stoichiometric,

ER>1, the mixture is fuel rich

ER<1, the mixture is fuel lean

The equivalence ratio is calculated by comparing the actual number of moles of fuel-to-oxidizer ratio to the stoichiometric fuel-to-oxidizer ratio shown in Eq. (5) where *F* is the number of moles of fuel and *A* is the number of moles of oxidizer.

$$\mathbf{ER} = \frac{\mathbf{F/A_{actual}}}{\mathbf{F/A_{stoich}}} \qquad (5)$$

For example, the general hydrocarbon case shown above would yield an equivalence ratio shown in Eq. (6).

$$\boldsymbol{ER} = \frac{\mathbf{a/(x+(\frac{y}{2})_{actual}}}{\mathbf{e/(x+(\frac{y}{2})_{stoich}}} = \mathbf{1\ for\ a = e} \quad (6)$$

Equation (6) shows that for *a*=*e*, the mixture is stoichiometric. The mixture will be fuel lean is *a*<*e* and fuel rich if *a*>*e*.

Although hydrocarbon combustion is used for the example here, the same principles apply to the solid combustion that is presented in this work. Maintaining stoichiometry is critical when varying other parameters so to not change the fundamental combustion.

Aluminum Combustion

The fuel of interest in this work is aluminum (Al). Aluminum combustion is widely studied due to its high heats of combustion and energy density. The energy density of metal fuels is much higher than that of monomolecular explosives (meaning that they have the fuel and oxidizer in the same molecule (i.e., TNT)).

The oxidative reaction that takes place converts the metal (Al) to the metal oxide (Al_2O_3). Aluminum particles are spherical and they contain a native oxide layer that is typically 3-5 nm in thickness.

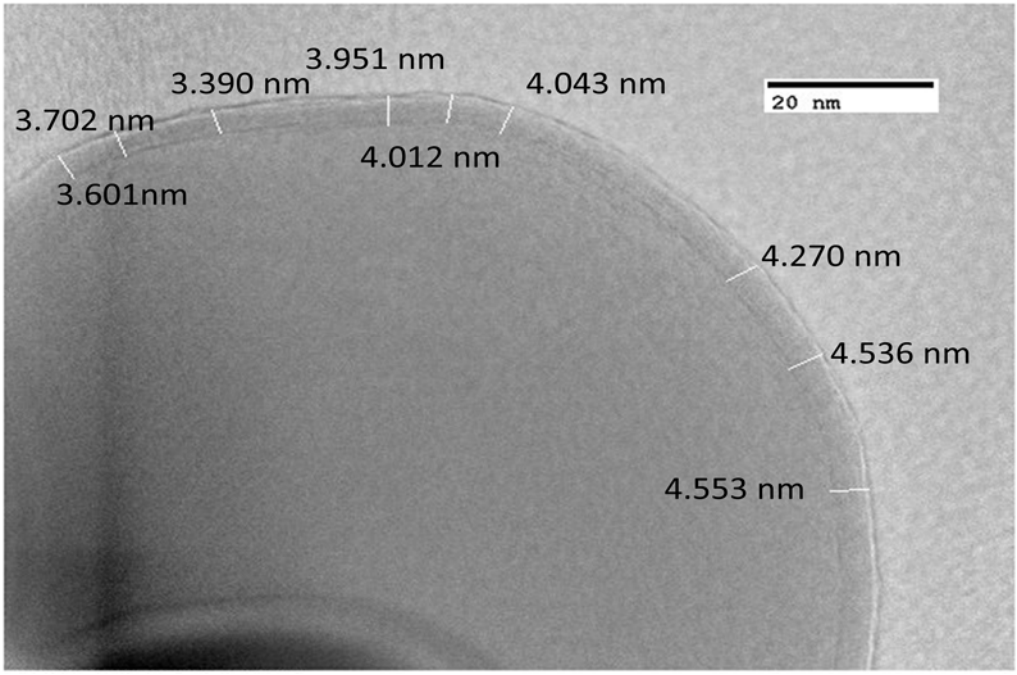

Figure 2. Transmission electron spectroscopy (TEM) image of a nano-scale Al particle to show alumina shell thickness. The average thickness is 4.01 nm. This thickness was used in the purity calculations for micron-scale Al particles (< 1% by mass oxide).

Aluminum is pyrophoric, so this passivation layer stabilizes the particles and allows them to be handled in oxygen-rich and moisture containing environments.

When Al is blended with metal oxides and heat is applied, Al receives oxygen from the metal oxide and results in aluminum oxide (also known as

alumina or Al_2O_3). This reaction is shown in the simplified chemical equation shown in Eq. (7).

$$2Al + 3CuO \rightarrow Al_2O_3 + 3Cu \quad (7)$$

Aluminum is also very reactive with fluorine. Fluoropolymers (i.e., polytetrafluoroethelyne (PTFE)) can be used as an oxidizer and the product expected is aluminum fluoride (AlF_3). A simplified version of this reaction is shown in Eq. (8).

$$4Al + 3C_2F_4 \rightarrow 4AlF_3 + 6C \quad (8)$$

Perfluoropolyether (PFPE)

Perfluoropolyether (PFPE) is a lubricant that is used for high performance automotive and aerospace applications due to its ability to withstand high temperatures (< 316 ^oC). Unless in the presence of a degrading metal (i.e., Al), PFPE is chemically inert. The chemical structure of PFPE is shown in Fig. 3.

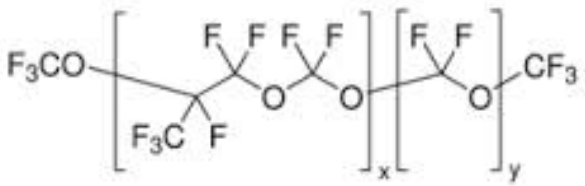

Figure 3. The chemical structure of PFPE.

Unlike PTFE which is a fluoropolymer, PFPE is a fluorooligomer which is a fluoropolymer intermediate consisting of only a few structural units. This allows PFPE to have different molecular weights based on chain length.

Pre-ignition Reaction

For Al-based thermites, when fluorine replaces oxygen as the reducing agent, aluminum fluoride (AlF_3) is formed instead of Al_2O_3. Both AlF_3 and Al_2O_3 are comparably thermodynamically stable with heats of formation of 1510 kJ/mol and 1676 kJ/mol, respectively. However, AlF_3 formation is preferred to Al_2O_3, because Al-F (664±6 kJ/mol)(Cottrell 1958) bond formation is stronger than the Al-O bond (512±4 kJ/mol)(Cottrell 1958). In fact, F has been shown to react with the alumina passivation shell surrounding an Al particle to form AlF_3(Osborne and Pantoya 2007). The exothermic surface reaction precedes the main Al oxidation reaction and has been coined a pre-ignition reaction (PIR)(Osborne and Pantoya 2007). Figure 4 shows a DSC curve for an Al-PTFE reaction.

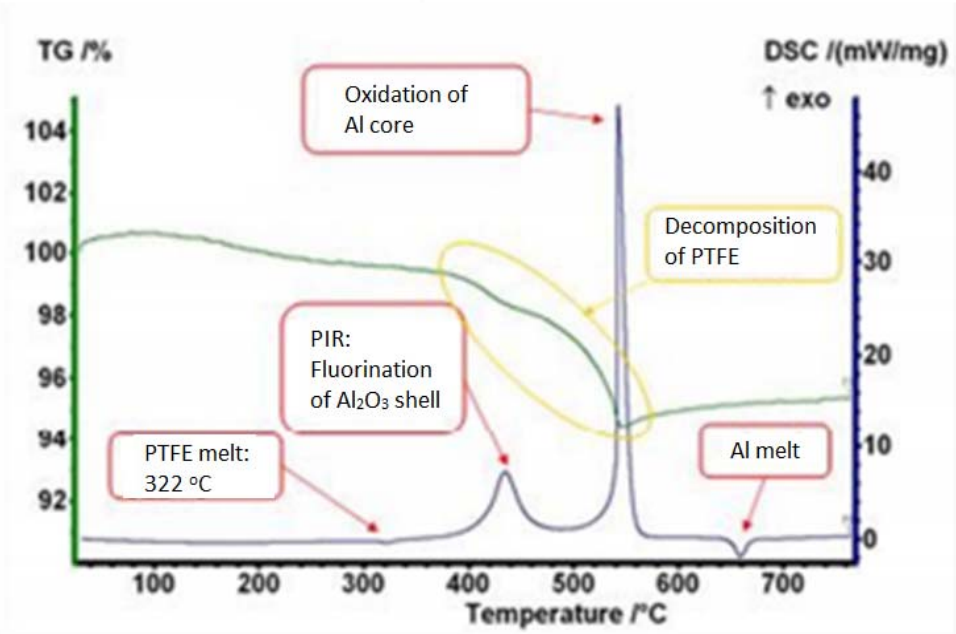

Figure 4. Heat flow and mass loss curves for the Al-PTFE reaction. Note the exotherm that occurs at the decomposition temperature of PTFE.

The PIR is a small but prominent exothermic peak that coincides with the decomposition temperature of PTFE and occurs before the oxidation of the Al core.

Metal Oxides

When Al particles react with metal oxides (i.e., molybdenum trioxide (MoO_3) or copper oxide (CuO)), the reaction is highly exothermic with flame temperatures exceeding 2000 K(Fischer and Grubelich 1998). This occurs because aluminum oxide has a higher heat of formation than other metal oxides (J. J. Moore and Feng 1995). Like Al, CuO has a spherical morphology but MoO_3 particles are flake structures. The differences in morphology are shown in Fig. 5.

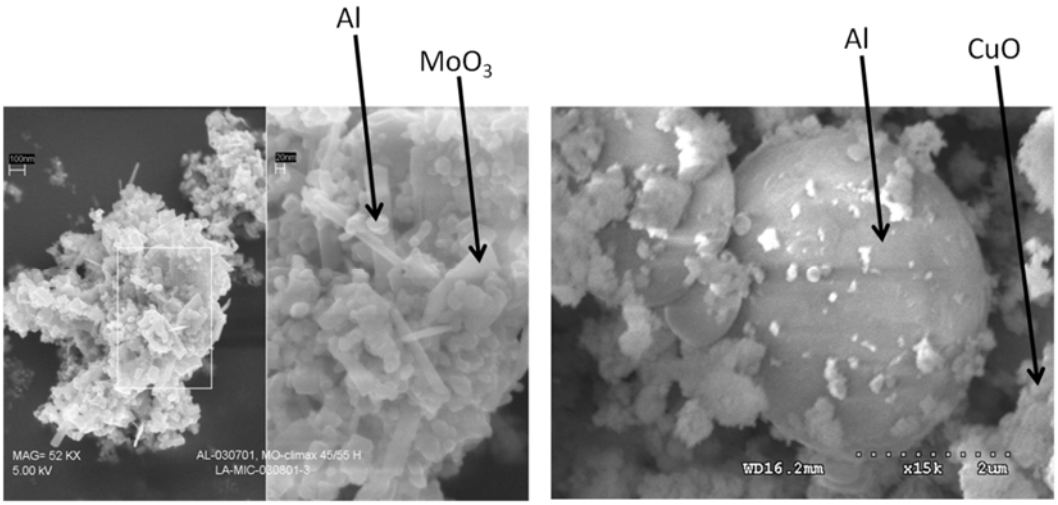

Figure 5. SEM images of Al with (a) MoO_3 and (b) CuO.

These highly reactive blends of metallic fuel and metal oxide are called thermites. Their applications range from material synthesis(Shigeta and Watanabe 2010; Deevi, Sikka, and Swindeman 1997; Yeh and Huang 2011) and alloying(C. Crane, Pantoya, and Dunn 2010; L. L. Wang, Munir, and Maximov 1993) to joining and welding(Iordachescu et al. 2010; Chen et al. 2006).

CHAPTER II: Activating Aluminum Particle Reactivity with Fluorine Oligomer Surface Coating

Abstract

Exothermic surface chemistry between fluorine and the alumina (Al2O3) shell surrounding aluminum (Al) fuel particles promotes aluminum reactivity. This study investigates the reactivity of Al when coated with a liquid fluorinated oligomer, specifically perfluoropolyether (PFPE). Flame speeds, differential scanning calorimetry (DSC), thermogravimetric analysis (TGA) and quadruple mass spectrometry (QMS) were performed for Al- PFPE blends with varying Al particle sizes (i.e., 80, 100, 120 and 5500 nm average diameter). The results show that the combustion performance of these blends is highly dependent on the Al2O3 concentration and exposed surface area. As Al particle diameter increases from 80 to 120 nm, the Al-PFPE blends exhibit an increase in flame speeds by 48%, but from 120 to 5500 nm, flame speeds decrease by 93%. There is a balance to optimizing Al particle reactivity with PFPE coating between activating Al particles with exothermic surface chemistry versus the unreacted alumina that contributes a thermal heat sink during energy generation. These results introduce a new and simplified synthesis approach for activating Al

particle surface chemistry to promote overall reactivity, and can be useful for many energy generation applications that involve aluminum combustion.

Introduction

Energetic blends of aluminum (Al) and fluorinated oxidizers such as polytetrafluoroethylene (PTFE) have been widely studied due to the unique surface exothermic chemistry between fluorine (F) and the alumina shell surrounding the Al particles which promotes Al reactivity. Fluorine is more electronegative than oxygen ($\chi_{p,oxygen}$=3.4 and $\chi_{p,fluorine}$=4.0)(Atkins and de Paula 2010) , and the Al-F bond is one of the strongest in nature (i.e. 664±6 kJ/mol(Cottrell 1958)). When Al reacts with F, AlF_3 is formed. The exothermic reaction has been observed by differential scanning calorimetry and associated with the identification of a small but prominent exothermic peak prior to the primary reaction(Osborne and Pantoya 2007; M. L. Pantoya and Dean 2009; Travis. R. Sippel, Son, and Groven 2013; Travis R. Sippel, Son, and Groven 2013; Miller et al. 2013; Farley et al. 2013). This peak has been coined a pre-ignition reaction (PIR) whose onset temperature is dependent on particle size (M. L. Pantoya and Dean 2009), fluorine source (K. S. Kappagantula et al. 2012; Farley et al. 2013) and equivalence ratio (Miller et al. 2013).

Typically the Al oxide shell is considered dead weight in a thermite reaction because it acts as a heat sink. By adding a fluorinated component, (such as PTFE) the shell undergoes exothermic surface chemistry which improves Al reactivity and contributes to the overall calorific output of the reaction (Osborne and Pantoya 2007; K. Kappagantula, Pantoya, and Hunt 2012; M. L. Pantoya and Dean 2009; Losada and Chaudhuri 2010; Conner and Dlott 2012) . Solid PTFE introduces a limit to the fuel-oxidizer contact surface area which limits the combustion performance in these diffusion controlled reactions(K. S. Kappagantula et al. 2012). In an attempt to resolve the limitation caused by fuel-oxidizer contact surface area, Kappagantula et al(K. S. Kappagantula et al. 2012) investigated the combustion of Al particles with surface functionalized self-assembled monolayers (SAM). The SAM consisted of perfluorotetradecanoic (PFTD) acid bonded to the aluminum particle's native oxide shell (Al_2O_3). Functionalizing Al_2O_3 with SAM is well documented with carboxylic(Oberg et al. 2001; M. Lee et al. 2007; Karaman, Antelmi, and Pashley 2001) and fluorinated acids(K. S. Kappagantula et al. 2012). This method involves chemically attaching acid chains to the surface hydroxyl layer on the alumina surface. The hydroxyl layer on Al_2O_3 is well studied and occurs naturally under standard atmospheric conditions(Peri 1965; Knoezinger 1978; Chupas and Grey 2004; Sarbak 1997).

Aluminum functionalized with PFTD successfully increased the reactivity of Al particles combined with MoO_3. In fact, the Al-PFTD composite particle combined with MoO_3 demonstrated 86% greater flame speeds than Al+MoO_3 for the same Al and MoO_3 particle size. Kinetic analysis using differential scanning calorimetry (DSC) revealed the Al-F pre-ignition reaction (PIR) for the functionalized Al particles not present in the Al without functionalization(Travis R. Sippel, Son, and Groven 2013; K. S. Kappagantula et al. 2012; Miller et al. 2013; Farley et al. 2013). The PIR induced an earlier onset of the main exothermic reaction, thereby promoting Al particle reactivity.

A simplistic approach for coating the Al surface is to introduce a liquid phase fluorooligomer that wets the Al particle surface. Miller et al.(Miller et al. 2013) studied this idea using a fluorinated oligomer to wet the surface of Al particles. The motivation was to suspend nano-scale Al particles in a structural epoxy-based matrix. To extend the shelf life of the Al particles, they applied PFPE as a protective coating because of its thermal stability at low temperatures (up to 316 ^{o}C in an oxygen-rich environment) and potential to produce exothermic activity beyond 316 ^{o}C (Miller et al. 2013).They studied the exothermic behavior for Al-perfluoropolyether (PFPE) blends of varying weight percents using differential scanning calorimetry (DSC) and found two exothermic peaks, one of

which occurred at the PFPE decomposition temperature of 316 ^{o}C. This first peak was identified as a pre-ignition reaction (i.e., PIR). They also found that the weight percent that produced the highest heat of combustion was 30% Al 70% PFPE corresponding to an equivalence ratio (ER) of 1.2 (i.e., slightly fuel rich).

Dean et al. analyzed DSC data for different Al_2O_3 particle sizes with PTFE in order to understand the role of exposed surface area on the exothermic Al-F reaction(M. L. Pantoya and Dean 2009). They found that the onset and magnitude of the PIR varied with particle size and exposed surface area for Al_2O_3 average particle sizes of 15, 30, 40 and 50 nm. They observed a decrease in PIR magnitude as Al_2O_3 particle size decreased from 50 to 30 nm and an increase in magnitude at 15 nm. Their results suggest an optimum Al particle diameter for promoting the Al-F surface exothermic chemistry is about 50 nm.

All of these studies(Osborne and Pantoya 2007; M. L. Pantoya and Dean 2009; Travis R. Sippel, Son, and Groven 2013; K. S. Kappagantula et al. 2012; K. S. Kappagantula, Pantoya, and Horn 2013; Farley et al. 2013) highlight Al-F reactions are: (1) exothermic; (2) a function of exposed Al_2O_3 surface area; (3) a function of the fluorine source (i.e., PFTD, PTFE); and (4) can activate Al reactivity with earlier onset of the main exothermic reaction. The objective of this study is to synthesize Al-PFPE formulations on a larger scale and analyze the macroscopic combustion

characteristics of the Al-PFPE reaction. This study extends the work by Miller et al.(Miller et al. 2013) who examined small (i.e. 5 mg) Al-PFPE samples for thermal equilibrium studies. All blends were prepared for a constant ER (φ=1.2). Flame speeds, DSC, thermogravimetric analysis (TGA), and quadruple mass spectrometry (QMS) was performed and analyzed for all blends in order to characterize combustion dynamics and reactivity.

Materials

Four different Al particle sizes were used and summarized in Table 1. Images obtained for 80, 100 and 120 nm Al particles by transmission electron microscopy (TEM) are shown in Fig. 6.

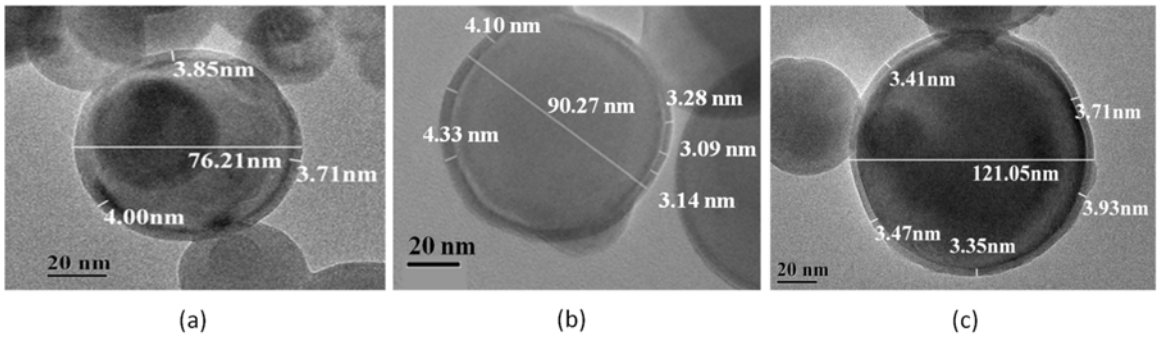

Figure 6. TEM representative for Al particles with average diameters of (a) 80 nm, (b) 100 nm, (c) 120 nm.

Each particle was passivated by an approximately 3.7 nm thick alumina shell as characterized by TEM analysis (Fig. 6). Due to thickness limitations with

TEM, the micron-scale particles could not be measured in this way. Instead, their size was examined using an AccuSizer 780 Optical particle size analyzer (Santa Barbara, CA). The micron-scale Al was suspended in filtered water (2mg Al/80 ml water) and sonicated for 60 minutes in cycles of 10 seconds on, 10 seconds off in order to avoid heating. The sample was then pulled using a syringe pump into the size analyzer for measurement. Particle length (diameter) is calculated and plotted as a count-based measurement (i.e., number of particles with a given diameter, in µm units). This plot is shown in Fig. 7 and the size data is given in Table 1.

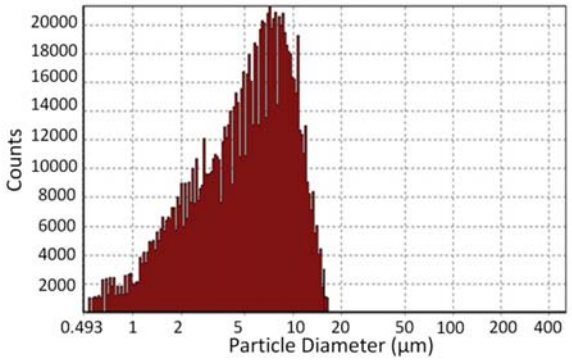

Figure 7. Particle size distribution for the micron-scale Al particles represented in number of particles with x diameter (i.e., counts).

Because the oxide layer thickness is independent of Al particle size, the oxide thickness used for purity calculations was estimated at 3.7 nm (i.e., the average of the other 3 samples).

The 80 and 120 nm average diameter Al particles were procured from Nanotechnologies (Houston, TX), the 100 nm average diameter Al was from U.S. Nanomaterials (Houston, TX) and the 5500 nm average diameter Al from Alfa Aesar (Ward Hill, MA). The PFPE (Fomblin® Y LVAC 25/6, average molecular weight of 3300 g mol^{-1}) was procured from Sigma Aldrich (St. Louis, MO).

Experimental Section

Equivalence ratio (ER) of 1.2 (i.e., slightly fuel rich) was maintained for all samples. An equivalence ratio is the balance for fuel (i.e. Al) and oxidizer (i.e. PFPE) in an energetic blend as shown in Eq. (9) where *M* is mass and *fuel* is Al, and *oxidizer* is PFPE.

$$ER = \frac{\left[\frac{M_{fuel}}{M_{oxidizer}}\right]_{actual}}{\left[\frac{M_{fuel}}{M_{oxidizer}}\right]_{stoichiometric}} \qquad (9)$$

When the reaction completes with no remaining fuel (Al) or oxidizer (PFPE) in the products, it is stoichiometric (i.e., ER=1). The reaction of Al and PFPE is

shown in Eq. (10) where *E* represents other products of the reaction and *a, b* and *c* are the constants used to balance the reaction.

$$aCF_3O\text{-}[\text{-}CF(CF_3)CF_2O\text{-}]_x(\text{-}CF_2O\text{-})_yCF_3 + bAl \rightarrow cAlF_3 + E \quad (10)$$

The reaction was balanced in this manner for all particle sizes to account for the Al and Al_2O_3 respective concentrations. The alumina concentrations range from 23 to 36 mass percent for 120 to 80 nm respectively and less than 1 mass percent for the micron-scale Al particles.

Miller et al. prepared the Al-PFPE blends by hand mixing with a spatula for five minutes(Miller et al. 2013). Due to the small sample size required for DSC analysis (i.e., 5 mg), this mixing method is sufficient. However, the level of PFPE dispersion needed for analyzing energy propagation of larger quantities (i.e., 300 mg) required a modified mixing technique. A fluorinated solvent for mixing was included here which improved dispersion needed for energy propagation analysis. The fluorine in the solvent disperses the fluorine in the PFPE and suspends the Al particles to promote better coating. The solvent used in this study was Perfluorosolv-2 (PFS-2) from SPI supplies (West Chester, PA). In order to flow into the sample holders, 100 ml of solvent was used per 300 mg of Al-PFPE. The solvent, Al and PFPE were mixed in a Thinky (Tokyo, Japan) planetary mixer for 3 minutes at 1500 RPM.

Flame Speed Experiments

Due to the dramatic change in Al particle surface area between sizes, the powders reclaim with a different consistency. In order to mitigate this, an acrylic apparatus was machined with two notches (see Fig. 8).

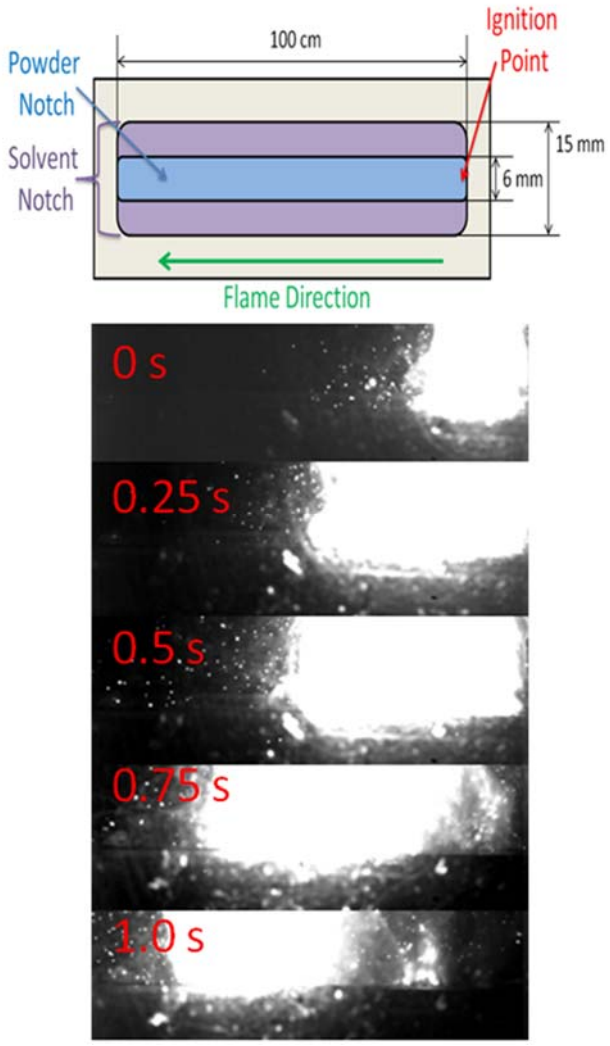

Figure 8. Schematic of the acrylic sample holder used for drying and igniting Al-PFPE blends and time-stamped representative still frames to illustrate Al-PFPE burning behavior.

The large notch was designed to capture the excess solvent. While drying, the Al particles and PFPE settle into the smaller sub-notch. The sample mass was monitored until the solvent mass evaporated. Once dry, the bulk density of the samples ranged between $1.78\text{-}2.00$ g/cm^3. Percent theoretical maximum density (TMD) was calculated for each sample and is shown in Table 1.

Table 1. Material Specifications for Al Fuel Particles.

name **(nm)**	average particle size (nm)	oxide layer thickness (nm)	particle mass alumina (%)	TMD (g/cm^3)	Bulk Density (g/cm^3)	%TMD (%)	Specific Surface Area (1/cm)
80	76	3.9	36%	2.3	2.00	87	$7.9x10^5$
100	91	3.6	29%	2.2	1.96	90	$6.7x10^5$
120	121	3.6	23%	2.2	1.93	95	$5.0x10^5$
5500	5800	3.7	<1%	2.1	1.78	96	$1.2x10^4$

For flame propagation analysis, one end of the open notch was fitted with a nickel-chromium wire for ignition. Each sample contained 300 ± 10 mg of Al-PFPE blend. The trays were loaded into a blast chamber which was fitted with an acrylic viewing window. The experimental setup is shown in Fig. 9.

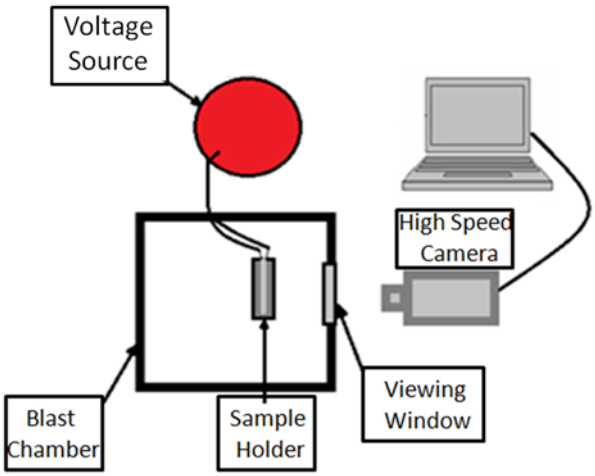

Figure 9. Ignition setup for tracking energy propagation.

The Al-PFPE blends were ignited by hot wire and the flame propagated along the length of the tray. The reaction was captured using a Phantom v7 (Vision Research, Inc., Wayne, NJ, USA) fitted with a Nikon AF Nikkor 52 mm 1:2.8 lens with an F-stop of 32. The camera was placed perpendicular to the reaction path and collected data with a resolution of 800 x 512 pixels at 1000 frames per second. The reaction is captured as a series of images which are then analyzed using NI Vision Builder to obtain the change in position of the flame front as a function of time. Each reported flame speed is the average of five experiments and the uncertainty in the measurement is represented by the bars in Fig. 10. The uncertainty is <10% such that this method was successful in producing macroscopically dispersed Al-PFPE mixtures in terms of repeatable energy propagation behavior and measurements.

Equilibrium Analysis

Simultaneous Thermal Analysis (STA) was performed using a Netzsch Jupiter STA 449 differential scanning calorimeter and thermogravimetric analyzer (DSC/TGA). The samples were heated at 5, 10 and 15 ^{o}C/min from room temperature to 700 ^{o}C in an environment comprised of 20% O_2/80% Ar by volume. Approximately 15 mg samples were loaded into crucibles and placed into the STA. Sintering can occur during heating and melting, ultimately affecting heat transfer in the STA measuring head. To ensure consistency, repeatability and minimize artifact alterations of results, four experiments were performed for each sample. Temperature calibrations for the instrument were performed using melting of a set of metal standards resulting in a temperature accuracy of ±1^{o}C.

During the STA thermal cycle, gas species were identified using a Netzsch Aeolos 403 C quadruple mass spectrometer in order to probe for the onset and relative magnitude of hydrogen fluoride (HF) gas. Probes were programmed to collect the following masses: HF (19), H_2O (18), CO_2 (44), CF_2 (50) and CF_3 (69) but only significant values of HF were detected. Each spectrum is loaded into the analysis program as a gas signal as a function of temperature where onset and magnitude can be identified.

Adiabatic flame temperature simulations for all samples were calculated using REAL code (Timtec L.L.C.). Using this thermal equilibrium software model, adiabatic flame temperature (T_f) was calculated assuming a constant pressure of 101.325 MPa and internal energy equal to zero kJ/kg. These T_f values are an upper limit for the ideal case of complete combustion. Kappagantula et al. used this software to calculate adiabatic flame temperature and their calculated values showed good agreement with their measured values for T_f (K. Kappagantula, Crane, and Pantoya 2013; K. Kappagantula, Crane, and Pantoya 2014).

Results

Flame speed results are shown in Fig. 10 and Table 2. The results show an increase of 48% from 80 nm to 120 nm and a decrease of 86% for the micron-scale Al particle size.

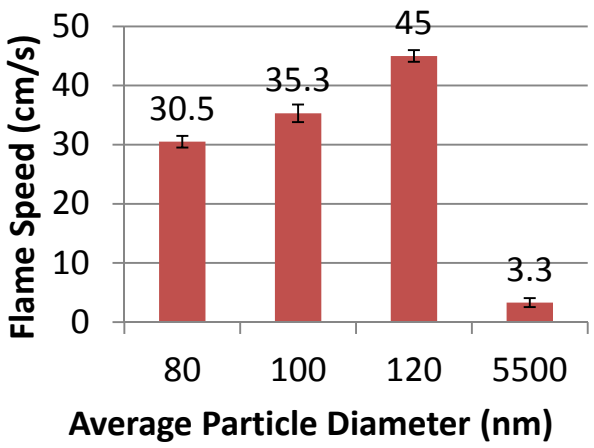

Figure 10. Flame speeds and activation energies for Al-PFPE as a function of Al particle size, equivalence ratio held constant and environment is air at standard temperature and pressure.

Table 2. Adiabatic flame temperature, exothermic peak temperatures for different DSC heating rates and calculated activation energy for all Al-PFPE samples.

Al diameter (nm)	Adiabatic flame temperature (K)	Peak Temperature at 5 KPM (°C)	Peak Temperature at 10 KPM (°C)	Peak Temperature at 15 KPM (°C)	Activation Energy (kJ/g)	Flame Speed (cm/s)
80	3900	767.7	670.0	593.8	1.53	30.5
100	3954	816.4	672.6	593.2	1.42	35.3
120	3992	819.7	677.1	589.2	1.39	45.0
5500	4063	810.0	673.6	636.3	1.72	3.3

Figure 11 shows the heat flux curves as a function of temperature for all particle sizes.

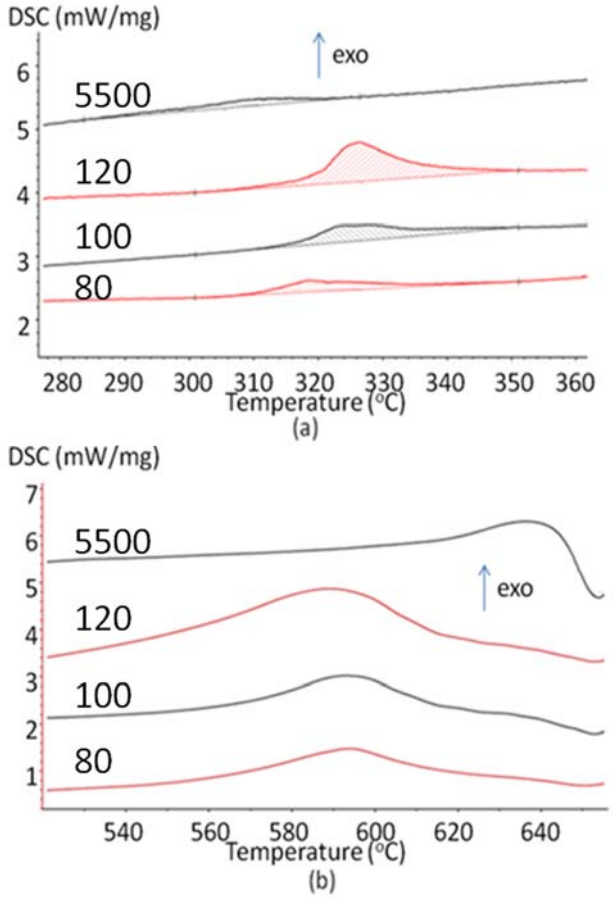

Figure 11. DSC curves of the (a) pre-ignition reaction and (b) main reaction for Al-PFPE blends, Al particle diameter=80,100,120, 5500 nm in 20% O_2/80% Ar by volume. Heating rate is 15 KPM for all data presented. Data reporting specific energy for each exotherm.

The exotherms for the PIR and main reaction increase as particle size increases from 80 to 120 nm and both exotherms decrease for the micron scale samples (see Table 3 for values).

Table 3. Magnitude and onset of exotherms, gas curves and mass loss for each sample.

Al diameter	PIR	PIR onset	main reaction	main reaction onset	mass loss	F gas signal per mg PFPE	Gas Signal Onset
(nm)	(J/g)	(^{o}C)	(J/g)	(^{o}C)	(%)	(A*s/mg)	(^{o}C)
80	19.6	315.6	123.5	558.5	-68.9	27.1	351.0
100	19.8	314.7	132.5	560.8	-68.8	26.7	341.7
120	21.0	312.9	146.2	564.0	-68.8	23.9	349.9
5500	7.3	313.4	73.0	618.2	-57.2	20.0	363.1

The onset for the micron-scale main reaction is about 60 ^{o}C higher than the main reactions for the nano-scale reactions. These results show that micron-scale Al is less reactive than nano-scale counterparts and this has been seen by others(Levitas, Dikici, and Pantoya 2011; Hunt et al. 2009; M. Pantoya and Granier 2005; Hunt and Pantoya 2005).

Figure 12a shows gas species evolution for HF liberation in each sample. It is noted the signals for H_2O, CO_2, CF_2 and CF_3 only account for 2% of the total gas signal. The area under each curve (Fig. 12a) was normalized to the mass of PFPE in the systems and that data is shown in Fig. 12b. The normalized gas signal decreases as particle size increases (i.e., as the alumina concentration decreases).

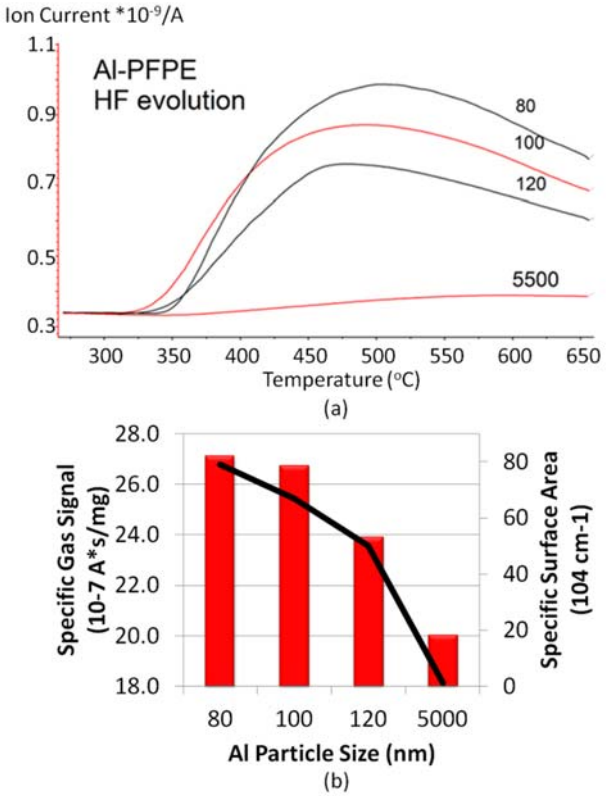

Figure 12. (a) HF gas evolution for 80, 100, 120 and 5500 nm Al with PFPE and (b) gas signal per mg of PFPE in each sample. The amount of HF liberated from each sample decreases as particle size increases (i.e., as alumina content decreases).

Table 2 shows the adiabatic flame temperatures calculated via thermal-equilibrium software. As particle size increases from 80 to 5500 nm, the adiabatic flame temperature increases from 3900 to 4016 K.

Activation energy is calculated from the DSC curves using the isoconversion method in Eq. (11)(K. S. Kappagantula et al. 2012; Hunt and Pantoya 2005; Farley et al. 2013), where *B* is the DSC heating rate (5, 10, and 15

Kelvin per minute (KPM)) and T_p is the temperature of the peak of the exothermic reaction (given in Table 2).

$$\ln\left[\frac{B}{T_p^{1.95}}\right] = -\frac{E_a}{RT_p} + lnA \qquad (11)$$

By measuring T_p for three heating rates, E_a can be extrapolated from the slope for a mixture (see Fig. 10).

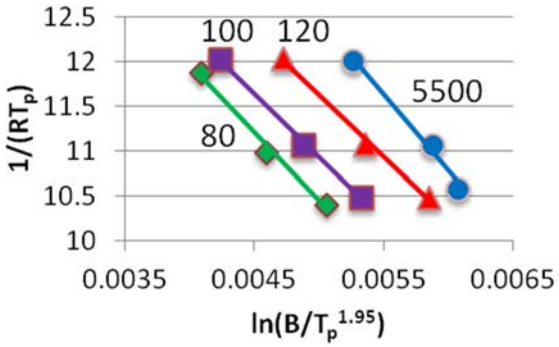

Figure 13. Trend lines showing activation energy for each particle diameter Al-PFPE samples. Activation energies are reported in Table 2.

This and similar proposed methods for calculating activation energy have been used by others(Kissinger 1957; Ozawa 1992; Boswell 1980; Starink 1996; Dyer and Munir 1995).

Discussion

Figure 10 shows that the fluorinated coating is significantly more reactive with nano-scale Al particles than micron scale. This may be associated with the

exposed Al_2O_3 surface area of each sample. The Al particles are spherical and the specific surface area (1/nm) can be calculated by Eq. (12).

$$\boldsymbol{A_{sp}} = \frac{\mathbf{4}\pi \boldsymbol{r}^{\mathbf{2}}}{\frac{\mathbf{4}}{\mathbf{3}}\pi \boldsymbol{r}^{\mathbf{3}}} = \frac{\mathbf{3}}{\boldsymbol{r}} \qquad (12)$$

The magnitude of the PIR increases in nano-Al-PFPE as specific surface area decreases (Tables 1 and 3). Also, the magnitude of the PIR correlates with flame speed (Fig. 10 and 11a): larger nano-Al particles produce faster flame speeds with PFPE. This correlation implies that optimizing the calorific output from the PIR can lead to enhanced energy propagation. Once the average particle size reaches the micron-scale (i.e., 5500 nm Al), flame speeds decrease, in part, due to insufficient alumina present to catalyze PFPE decomposition.

The flame speed trends (Fig. 10) also follow closely with the main reaction exotherm magnitude, specifically; higher flame speeds correspond to larger exotherms. These results (Fig. 11b) suggest a correlation between calorific output and energy propagation, implying a dominant role of conductive energy propagation. These blends are highly consolidated mixtures with bulk density ranging from 87 to 92 %TMD such that porosity is limited to 13-8% of the solid volume. For these high density blends convective energy transport is more limited and conduction is dominant. The samples with larger magnitude PIR and

main reactions may provide more energy for conductive heat transfer thereby exhibiting high flame speeds.

Activation energies for all Al-PFPE blends correlate well with the inverse of the measured flame speeds (see Table 2). As activation energy decreases, flame speed increases suggesting flame speed is a function of the reaction kinetics as well as the conductive mode of energy propagation.

Because the PIR is highly controlled by the specific surface area, a way to investigate the extent of the surface chemistry is to vary the aluminum particle size, and therefore exposed surface area. As the specific surface area increases (i.e. particle size decreases), the available sites for Al-F surface reactivity increase. Kasai et al. showed that alumina is a good catalyst for PFPE decomposition[14]. Because the mixtures were blended to a constant stoichiometry, the alumina concentration increases as particle size decreases. This is why decreasing Al particle size produces an increase in specific HF gas production (see Fig. 12). The PFPE is exposed to more alumina surface area and undergoes better decomposition with the 80 nm particle size. Because the equilibrium analysis and open tray burns allow for much of the HF gas to escape the system, much of the fluorine that would catalyze surface combustion has left the system prior to energy propagation. The decrease in performance in the micron-Al-PFPE may be

caused, in part, by the higher activation energy allowing appreciable HF gas escape prior to particle ignition and energy propagation.

Conclusion

Flame speeds, differential scanning calorimetry (DSC), thermogravimetric analysis (TGA) and quadruple mass spectrometry (QMS) were performed for Al-PFPE blends with varying Al particle sizes (80, 100, 120 and 5500 nm in average diameter). The results show that the combustion performance of these blends is highly dependent on the Al_2O_3 exposed surface area. High specific surface area associated with nano-Al particles catalyzes AlF_3 formation via exothermic surface chemistry. This reaction promotes the decomposition of PFPE (as seen by higher HF gas evolution), and provides greater overall calorific output for diffusive energy propagation, as seen in the higher flame speeds for nano-Al-PFPE blends. Activation energy was also measured and found to inversely correlate with flame speed indicating that reaction kinetics also play a dominant role in improving combustion performance. These results provide a new direction for activating Al particles towards greater reactivity: by including a fluorinated oligomer to exploit exothermic surface reactions contributing toward overall energy generation.

CHAPTER III: Activating Aluminum Reactivity for Improved Energetic Composite Combustion

Abstract

Energetic blends of nanometer-sized aluminum (Al) particles with liquid perfluorocarbon-based oxidizers such as perfluoropolyethers (PFPE) excite surface exothermic chemistry between fluorine and the alumina passivation shell surrounding an Al core particle that promotes Al reactivity. Many Al fueled energetic composites use solid oxidizers that induce no alumina surface exothermicity, such as molybdenum trioxide (MoO3) or copper oxide (CuO). This study investigates a perfluorinated polymer additive, PFPE, incorporated to activate Al reactivity in Al-CuO and Al-MoO3. Flame speeds, differential scanning calorimetry (DSC) and quadruple mass spectrometry (QMS) were performed for varying percent PFPE blended with Al/MoO3 or Al/CuO in order to examine reaction kinetics and combustion performance. X-ray photoelectron spectroscopy (XPS) was performed to identify product species. Results show that the performance of the thermite-PFPE blends is highly dependent on the bond dissociation energy of the metal oxide. Fluorine-aluminum based surface exothermic chemistry with MoO3 produce an increase in reactivity while the blends with CuO show a decline when increasing the PFPE loadings. These results

provide new evidence that optimizing aluminum combustion can be achieved through activating exothermic Al surface chemistry that produces aluminum fluoride.

Introduction

A thermite is defined as an energetic system consisting of a metal fuel (i.e. aluminum (Al)) and metal oxide (i.e. copper oxide (CuO) or molybdenum trioxide (MoO_3))(Nixon et al. 2010; Gesner, Pantoya, and Levitas 2012; Fischer and Grubelich 1998; Hunt and Pantoya 2005). These systems are widely studied due to their high energy densities and heats of combustion(Cervantes et al. 2011; Yen and Wang 2012; Kyle T. Sullivan et al. 2010; M. Pantoya and Granier 2005; Hunt and Pantoya 2005; Sanders et al. 2014). As energy generating materials, thermite reactions have applications ranging from material synthesis(Shigeta and Watanabe 2010; Deevi, Sikka, and Swindeman 1997; Yeh and Huang 2011) and alloying(Charles a. Crane, Pantoya, and Dunn 2010; L. L. Wang, Munir, and Maximov 1993) to welding and joining(Iordachescu et al. 2010; Chen et al. 2006). Munir et al. present a thorough review on thermite applications(Dyer and Munir 1995),Fischer and Grublic tabulated thermo-chemical properties for hundreds of thermite reactions(Fischer and Grubelich 1998) and Koch presented chemistry and application of fluorocarbon-based energetics(Koch 2012).

For Al-based thermites, when fluorine replaces oxygen as the reducing agent, aluminum fluoride (AlF_3) is formed instead of Al_2O_3. Both AlF_3 and Al_2O_3 are comparably thermodynamically stable with heats of formation of 1510 kJ/mol and 1676 kJ/mol, respectively. However, AlF_3 formation is preferred to Al_2O_3, because Al-F (664±6 kJ/mol)(Cottrell 1958) bond formation is stronger than the Al-O bond (512±4 kJ/mol)(Cottrell 1958). In fact, F has been shown to react with the alumina passivation shell surrounding an Al particle (Osborne and Pantoya 2007). The exothermic surface reaction precedes the main Al oxidation reaction and has been coined a pre-ignition reaction (PIR)(Osborne and Pantoya 2007). Kappagantula et al. showed that the PIR can be used to enhance Al reactivity(K. S. Kappagantula et al. 2012).

Typically Al-fluoropolymer blends are prepared with a solid fluorinated oxidizer such as Teflon® (PTFE) (K. Kappagantula, Pantoya, and Hunt 2012; M. L. Pantoya and Dean 2009; Losada and Chaudhuri 2010; Conner and Dlott 2012) . Solid PTFE introduces a limit to the fuel-oxidizer contact surface area which is thought to limit the combustion performance(K. S. Kappagantula et al. 2012). In an attempt to resolve the limitation caused by fuel-oxidizer contact surface area, Kappagantula et al(K. S. Kappagantula et al. 2012) investigated the combustion of Al particles with surface functionalized self-assembled monolayers (SAM). The

SAM consisted of perfluorotetradecanoic (PFTD) acid bonded to the aluminum particle's native oxide shell (Al_2O_3). Surface functionalized Al-PTFD was successful in increasing the reactivity of Al particles combined with MoO_3 and produced an 86% increase in flame speed compared to Al-MoO_3 alone(K. S. Kappagantula et al. 2012). The enhancement in reactivity was attributed to the PIR resulting from the fluorine functionalization.

Another method for coating the Al surface that can be easily implemented is to introduce a liquid perflurorinated oligomer that phyisoabsorbs onto the Al particle surface. In a similar finding as Kappagantula et al., the liquid fluorooligomer may readily activate the PIR and promote greater overall Al reactivity. The liquid fluorooligomer used in this study is a class of viscous fluorinated oligomers called perfluoropolyethers (PFPEs). Miller et al. used a PFPE protective coating on nano-scale Al because of its thermal stability at low temperatures (up to 316 ^oC in an oxygen-rich environment) and potential to produce exothermic activity beyond 316 ^oC(Miller et al. 2013). When coated with PFPE, the Al particles were able to suspend in a structural epoxy-based matrix. Miller used differential scanning calorimetry (DSC) to study the exothermic behavior for Al-perfluoropolyether (PFPE) blends of varying weight percents. The DSC revealed two exothermic peaks, one of which occurred at the PFPE

decomposition temperature of 316 ^{o}C (i.e., the PIR). The 30% Al 70% PFPE blend produced the highest heat of combustion. This translated to an equivalence ratio (ER) of 1.2 (i.e., slightly fuel rich).

Previously, fundamental combustion analysis was performed for Al-PFPE blends(McCollum, Pantoya, and Iacono 2015). Flame speeds, differential scanning calorimetry (DSC), thermogravimetric analysis (TGA) and quadruple mass spectrometry (QMS) were performed for Al-PFPE blends with varying Al particle sizes (80, 100, 120 and 5500 nm in average diameter). The results showed that the combustion performance of these blends is highly dependent on the Al_2O_3 concentration and exposed surface area. As Al particle diameter increases from 80 to 120 nm, flame speeds increase by 48%, but from 120 to 5500 nm, flame speeds decrease by 93%. There is a balance to optimizing Al particle reactivity between activating Al particles with exothermic surface chemistry versus the unreacted alumina that contributes a thermal heat sink during energy generation. These results introduced a new and simplified synthesis approach for activating Al particle surface chemistry to promote overall reactivity.

The objective of this study is to use PFPE as an additive in different thermite systems (Al-MoO_3 and Al-CuO) in order to determine how the

perfluorinated oligomer affects reaction kinetics and overall reactivity. The metal oxides MoO_3 and CuO were selected based on their extensive use in research (Jian, Piekiel, and Zachariah 2012; H. Wang et al. 2014; K. Sullivan, Young, and Zachariah 2009; D. S. Moore, Son, and Asay 2004; Sanders et al. 2014) and their differing dissociation properties. Specifically, the dissociation energy for the Mo-O bond is 607±34 kJ/mol(Cottrell 1958) but the Cu-O bond energy is only 343±63 kJ/mol(Cottrell 1958). Using a PFPE coating in these thermite systems could extend their shelf life by limiting particle surface exposure to oxygen rich environments while exploiting exothermic surface chemistry with the alumina shell that may contribute to enhancing overall reactivity.

Experimental

Materials

Aluminum powder (100 nm average particle diameter) with 3 nm Al_2O_3 particle shell thickness was procured from U.S. Nanomaterials (Houston, TX). The PFPE (Fomblin® Y LVAC 25/6, average molecular weight of 3300 g mol^{-1}) and the CuO (50 nm average particle diameter (spherical)) powder was purchased from Sigma Aldrich (St. Louis, MO). The MoO_3 (44 nm average particle diameter (flake structures)) was received from Nanostructured & Amorphous Materials, Inc.

The composites were prepared to an equivalence ratio of 1.2 (i.e., slightly fuel rich). Equivalence ratio is shown in Eq. (13) where *M* is the mass and the *fuel* is Al, and the *oxidizers* are PFPE/CuO or PFPE/MoO_3.

$$\mathbf{ER} = \frac{\left[\frac{\mathbf{M_{fuel}}}{\mathbf{M_{oxidizer}}}\right]_{\mathbf{actual}}}{\left[\frac{\mathbf{M_{fuel}}}{\mathbf{M_{oxidizer}}}\right]_{\mathbf{stoichiometric}}} \qquad (13)$$

The equivalence ratio was maintained for all samples by performing a molar balance using Eq. (14) and Eq. (15) where *a, b, c, d* and *e* are coefficients used to balance each reaction and *H* represents other products of the reaction.

$$aCF_3O\text{-}[\text{-}CF(CF_3)CF_2O\text{-}]_x(\text{-}CF_2O\text{-})_yCF_3 + bAl + cMoO_3 \rightarrow dAl_2O_3 + eAlF_3 + H \qquad (14)$$

Or,

$$aCF_3O\text{-}[\text{-}CF(CF_3)CF_2O\text{-}]_x(\text{-}CF_2O\text{-})yCF_3 + bAl + cCuO \rightarrow dAl_2O_3 + eAlF_3 + H \qquad (15)$$

The PFPE concentration was calculated such that PFPE accounts for 0, 5, 10 and 20 wt. % of the reaction. The weight percent of each component are shown in Table 4.

Table 4. Weight percent of all components in each sample.

	Al	Oxidizer	PFPE
Al-CuO		CuO	
0	24%	76%	0%
5	23%	73%	5%
10	22%	69%	9%
20	21%	63%	16%
Al-MoO_3		MoO_3	
0	34%	66%	0%
5	34%	62%	4%
10	33%	59%	8%
20	32%	51%	17%

The PFPE, Al and CuO or MoO_3 were weighed and suspended in 60 ml of Perfluorosolv PFS-2™ from SPI Supplies (West Chester, PA). A fluorinated solvent for mixing was included in order to improve PFPE dispersion. The fluorine in the solvent disperses the fluorine in the PFPE and suspends the Al/CuO or Al/MoO_3 particles to promote better coating. The solution was then mixed using a planetary mixer at 1500 rpm for 2 minutes and poured into a Pyrex dish. The Perfluorosolv evaporated in a fume hood until the remaining mass was only that of Al/CuO/PFPE or Al/MoO_3/PFPE (about 24 h). Because of the high surface area of the Al/CuO and Al/MoO_3 and low concentration of PFPE, the samples reclaimed as loose powders.

Flame Speed Measurements

The powder was loaded into 3 mm inner diameter, 8 mm outer diameter, 10 cm long quartz tubes containing 300 mg of powder each (Fig. 14).

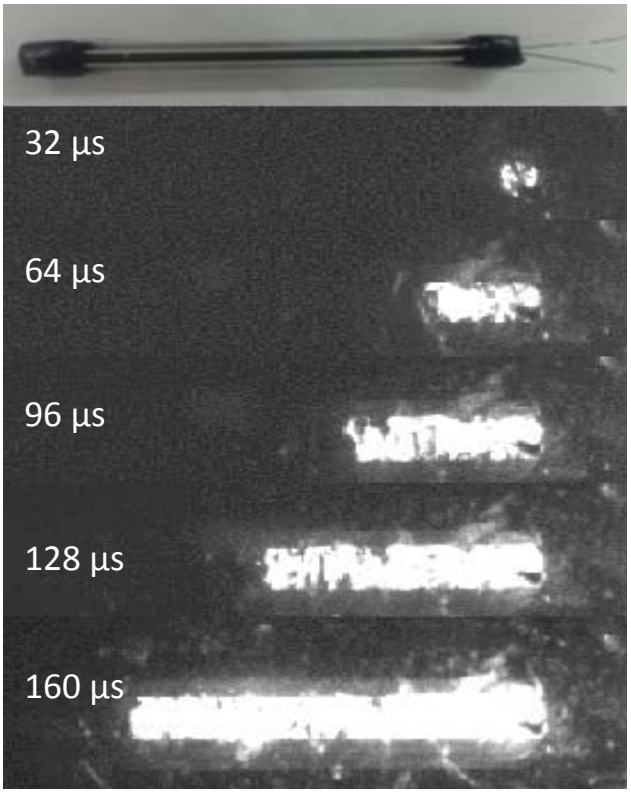

Figure 14. Representative still frame images time stamped of powder filled quartz tube and flame propagation. Bulk density is 10% theoretical maximum density and mixture is Al/MoO_3.

Both ends of the tube were sealed with one side securing a length of nickel-chromium wire, bent into a "V" shape and used for ignition by subjecting the wire to a voltage. Flame propagation was observed through a viewing window in the chamber. The reaction was recorded with a Phantom v7 (Vision Research, Wayne, NJ) high speed camera at a rate of 29,000 frames per second

and aligned perpendicular to the direction of flame propagation. The flame speed was determined by tracking the flame front through a referenced time and distance using the Vision Research Software. The resolution of the flame speed for this diagnostic is 0.1 m/s. Flame speeds were collected from five sets of experiments to ensure repeatability.

Thermal Equilibrium Analysis

Simultaneous Thermal Analysis (STA) was performed using a Netzsch Jupiter STA 449 differential scanning calorimeter and thermogravimetric analyzer (DSC/TGA). The samples were heated at 5 ^{o}C/min from room temperature to 1000 ^{o}C. Approximately 10 mg samples were loaded into crucibles and placed into the STA. Sintering can occur during heating and melting, ultimately affecting heat transfer in the STA measuring head. To ensure consistency, repeatability and minimize artifact alterations of results, five experiments were performed for each sample. Temperature calibrations for the instrument were performed using melting of a set of metal standards resulting in a temperature accuracy of ±1^{o}C.

Gas species were identified using a Netzsch Aeolos 403 C quadruple mass spectrometer in order to probe for the onset and relative magnitude of gaseous fluorine during the STA thermal cycle. Each spectrum is loaded into Netzsch Proteus software in order to identify species and magnitude as a function of

temperature. Probes were programmed to collect the following masses: HF (19), H_2O (18), CO_2 (44), CF_2 (50) and CF_3 (69). Because H_2O, CO_2, CF_2 and CF_3 only made up 2% of the total gas signal, the focus will be on HF.

X-ray Photoelectron Spectroscopy

X-ray photoelectron spectroscopy (XPS) was performed on the reaction products using a PHI 5000 Versa Probe with an Al Kα source. Samples were loaded in a vacuum chamber which was held to 10^{-6} Pa during measurement. Peaks were referenced to a C1s value of 284.8 eV. For the MoO_3-based thermite (MBT) samples, the survey spectra identified Al, Mo, O, F, and C. The CuO-based thermite (CBT) survey spectra identified Al, Cu, O, F, C and Na. Due to the presence of Na, analysis was performed on the O2s peak because the O1s peak was impeded by a Na1s peak.

Results and Discussion

Flame speed results for the two thermite systems as a function of PFPE concentration are shown in Fig. 15.

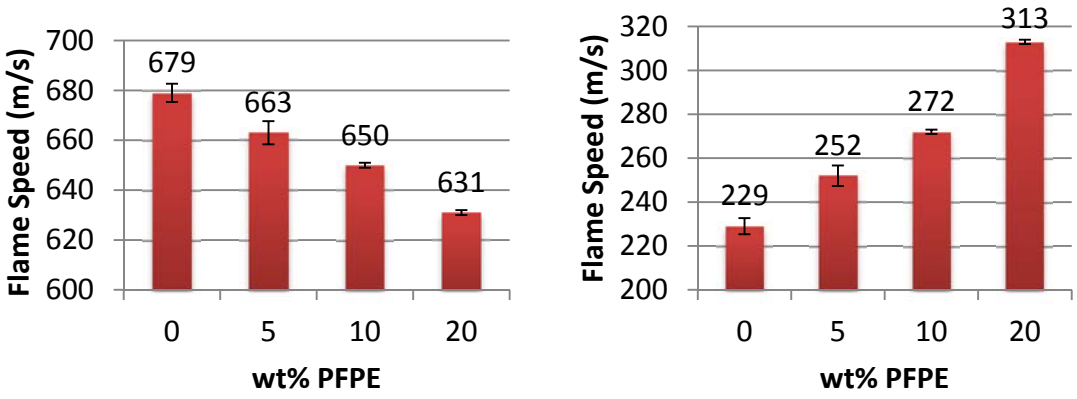

(a) (b)

Figure 15. Flame propagation velocity for aluminum with (a) CuO and (b) MoO_3 with varying percent of PFPE. Equivalence ratio remains constant for all mixtures.

Addition of PFPE yields different results with regard to oxidizing agent. The MoO_3-based thermites (MBT) benefit from the addition of PFPE, showing a continuous increase in flame speed (37% with the highest PFPE concentration). The CuO-based thermites (CBT) show the opposite trend: flame speed decreases as the PFPE concentration increases, with a decrease of 7% for the highest PFPE concentration.

The key question in this analysis is how fluorine from PFPE participates in the reactions. When combined with aluminum, the resulting product will be Al_2O_3 if Al reacts with oxygen reducing agents (i.e., CuO or MoO_3) and AlF_3 if Al

reacts with the PFPE. The equivalence ratio (Φ=1.2) was maintained with the addition of PFPE such that the oxygen and fluorine have equal availability to react with Al. Figure 16 shows the thermal analysis for 100 nm Al and PFPE alone. The results for onset and heat of combustion of each peak are shown in Table 5.

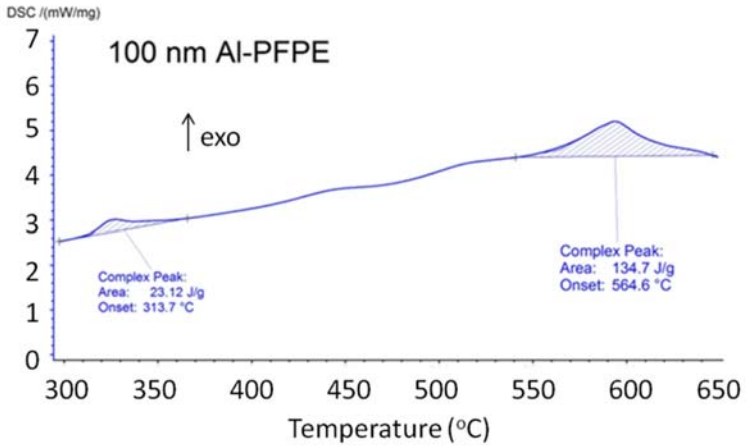

Figure 16. The oxidation reaction of 100 nm Al and PFPE heated from 35 to 1000°C at 5°C/min.

Table 5. Results for the DSC analysis of Al-CuO and Al-MoO_3 with x% of PFPE.

Sample	PIR Onset Temperature (^oC)	PIR ΔH_c (J/g)	Thermite Reaction Onset Temperature (^oC)	Thermite Reaction ΔH_c (J/g)
Al + PFPE	315	19.8	561	133
Al + CuO +0%PFPE	---	---	517	763
Al + CuO +5%PFPE	298	19.56	569	1658
Al + CuO +10%PFPE	299	29.70	581	1305
Al + CuO +20%PFPE	303	51.37	583	843
Al + MoO_3 +0%PFPE	---	---	508	2078
Al + MoO_3 +5%PFPE	298	21.79	534	1370
Al + MoO_3 +10%PFPE	301	35.17	541	1672
Al + MoO_3 +20%PFPE	305	103.1	566	1889

Figure 17 shows heat flow curves from thermal analysis for CBT and MBT from 280-380 ^{o}C. The magnitude of the CBT pre-ignition reaction (PIR) builds with PFPE loading (Fig. 17a), but is significantly less than that of the MBT (Fig. 17b). Also, the onset of the PIR is around 307 ^{o}C for both CBT and MBT. Table 5 shows the magnitudes of the PIR for each sample.

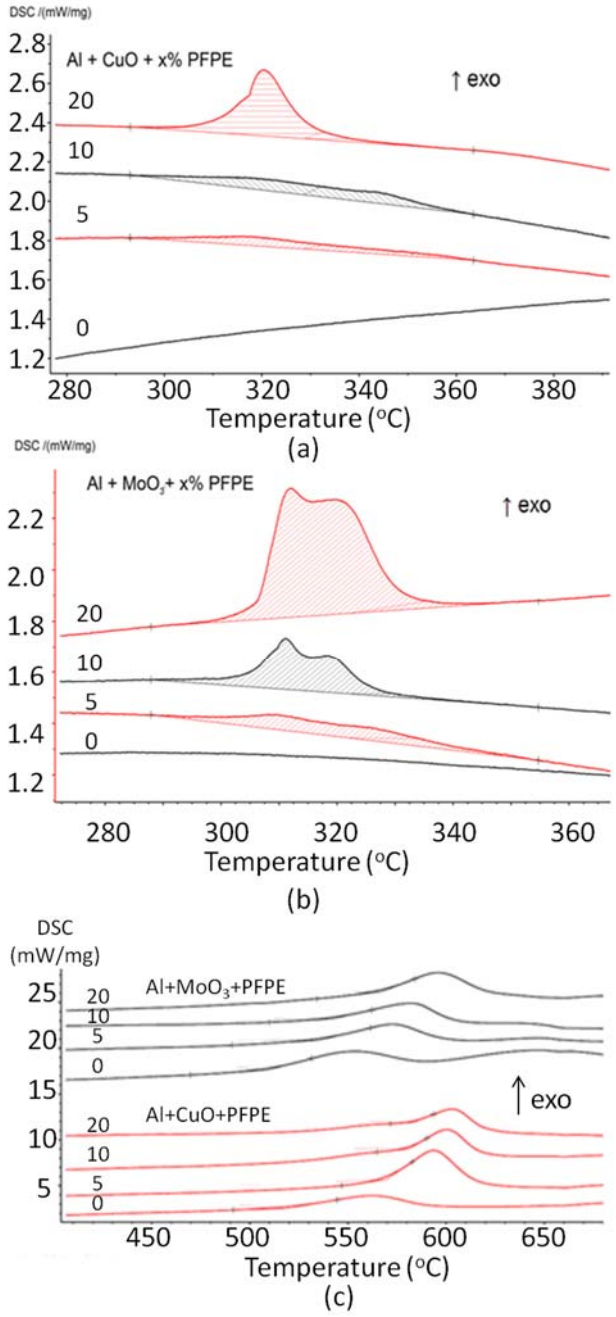

Figure 17. Pre-ignition reaction exotherm for aluminum with (a) CuO (PIR region) or (b) MoO_3 (PIR region) and (c) MBT and CBT (400-700 °C region). Samples were heated at 5 °C/min from 35°C to 1000°C in a 20% O_2/80% Ar by volume environment.

This low temperature exotherm has been identified by others and is associated with AlF_3 formation reactions(K. S. Kappagantula et al. 2012; Travis R. Sippel, Son, and Groven 2013; Miller et al. 2013; Farley et al. 2013).

The thermal analysis from 400-700^{o}C for all samples is shown in Fig. 17c and the results are summarized in Table 5. The onset temperature of the main reaction increases with both CBT and MBT as PFPE concentration increases. Also, the magnitude of the main reaction produces a continuously increasing heat of combustion (calculated as the area under the curve) with increasing PFPE for both metal oxide blends. As the amount of PFPE increases, both onset temperatures surpass the onset temperature for Al oxidation at 565 °C when heated with PFPE alone (Fig. 16). It is noted that PIR are not shown in Fig. 17c because the difference in magnitude between the PIR and main reaction is too large to distinguish the smaller PIR peaks.

From Figs. 15-17, an increase in flame speed was observed in for MBT, and MBT shows that the PIR grows in exothermicity as PFPE concentration increases (Fig. 15b). This suggests that fluorine contribution to the reaction increases as the PFPE concentration increases and this growing PIR may correlate to an increase in flame speed with PFPE concentration. In contrast, Figs. 15-17 shows CBT exhibits a decrease in flame speed with PFPE concentration and the PIR is

significantly smaller than that of the MBT samples (see Table 5). Without significant contribution from the early stage PIR (Table 5), chemical energy liberated from the reaction is delayed to higher onset temperature thereby limiting energy propagation and reducing flame speed.

The opposite trends in flame speed shown in Fig. 15 may depend on the bond dissociation energy (BDE) of the different metal oxidizers. The energy to break the Cu-O bond is only 343±63 kJ/mol but for the Mo-O bond it is 607±34 kJ/mol(Cottrell 1958). The fluorine received from the PFPE is bonded to carbon and the BDE of that bond is 536±21 kJ/mol(Cottrell 1958), the carbon-carbon bond is 607±21 kJ/mol(Cottrell 1958) and the carbon-oxygen bond is 1076.5±4 kJ/mol(Cottrell 1958). Crouse et al. suggested that a possible mechanism for Al_2O_3 catalyzed reaction with PTFE involves the chemisorption of a CF_2 radical(Puts and Crouse 2014). The energy needed to dislodge an oxygen atom from CuO to react with Al is significantly lower than the energy needed to extract fluorine alone from PFPE or to extract the CF_2 radical by breaking the C-C bond in the PFPE. For this reason, the PFPE reaction with Al may be overshadowed in the CBT because O is more readily available to oxidize Al (i.e., 343 vs. 607 m/s). However, when the blends are made with an oxidizer with a higher BDE (i.e. MoO_3), the PFPE has a greater chance to participate in the reaction because the

energy needed to extract fluorine (or CF_2 radical) and oxygen atoms from their respective reducing agents are similar. This can be confirmed by analyzing the products of the different reactions in order to identify the presence of AlF_3 in the different samples.

Hydrogen fluoride (HF) gas generation was monitored during thermal analysis and shown as a function of temperature in Fig. 18a and 18b. For CBT, HF gas evolution decreases with increasing concentration of PFPE. In contrast, MBT show greater HF gas evolution with increasing PFPE concentrations. Figure 17c shows the HF gas signal per mg PFPE (As/mg) for all samples.

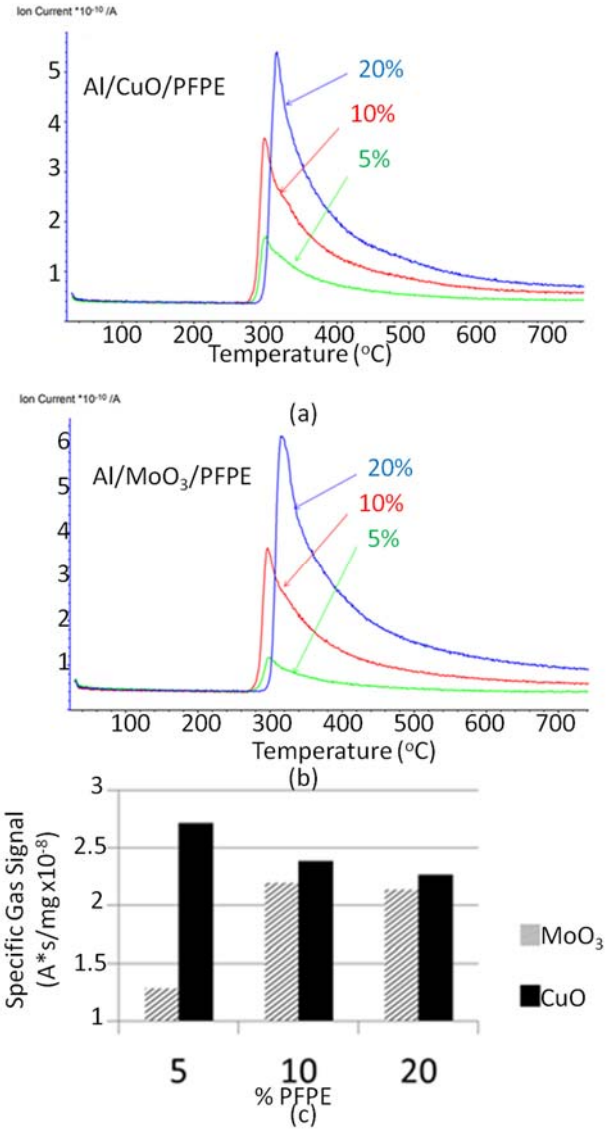

Figure 18. QMS curves for fluorine gas liberated from (a) CBT, (b) MBT and (c) gas evolution per mg PFPE. The MBT show an increase and limit in HF gas liberation while the CBT show a decrease.

The onset of HF gas release is approximately < 350 ^{o}C which corresponds to the decomposition of PFPE(Kasai, Tang, and Wheeler 1991). The CBT show a decrease in the release of HF per mg of PFPE which indicates that F bonds are either being formed with the other materials in the system, or that PFPE decomposition is hindered in some way. The normalized spectrum for the MBT show an increase in HF gas produced per mg PFPE from 5 to 10%, but there is little change from 10 to 20% PFPE concentration. This data suggests that more Al-F bonds are formed with the MBT than the CBT and is consistent with the magnitudes of the PIR in Fig. 17 and Table 5. Specifically, more exothermic PIR is consistent with more Al-F bond formation and lower HF gas evolution.

In order to identify how F bonds to each component in the combustion products, XPS was performed on products from the MBT and CBT reactions for 5% and 20% PFPE. Figure 19 shows the survey spectrum of the MBT samples (i.e., a. MBT5, b. MBT20) and CBT samples (i.e., c. CBT5 and d. CBT20).

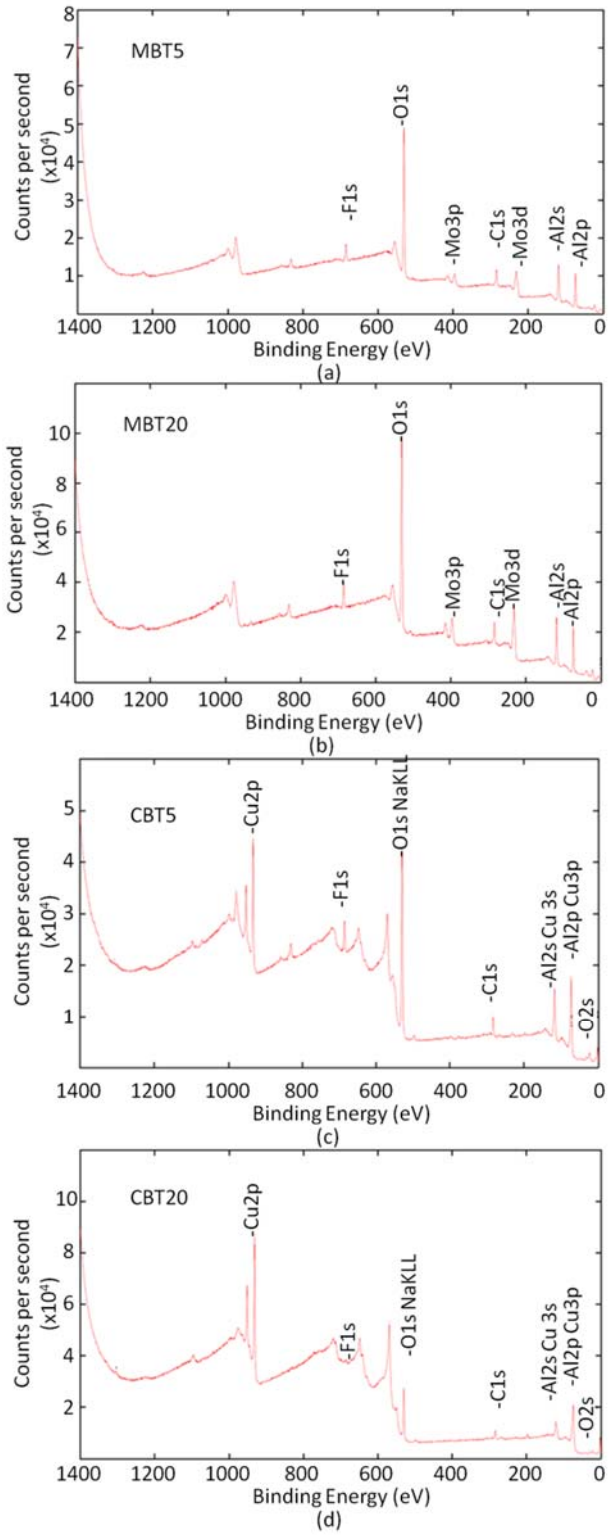

Figure 19. Survey Spectra for (a) MBT5 and (b) MBT20 (c) CBT5 and (d) CBT20.

The relative signal of fluorine decreases significantly from CBT5 to CBT20. (Note: The counts per second axis of the CBT samples are shifted in order to see the low intensity peaks in CBT20.)

Fluorine bonds are present for all samples. Inspection of these plots shows a comparable signal of every element in the MBT samples, but a drastic decline in F signal from CBT5 to CBT20. Upon closer inspection, Mo3d shows a greater number of pronounced peaks in the MBT5 sample versus MBT20. The peaks at 226 eV and 229 eV are metallic Mo 3d5/2 and 3d3/2 respectively (see Fig. 20)(Al-Kandari et al. 2013). Peaks at 228, 231, 232, and 235 are indicative of Mo-O bonds(Al-Kandari et al. 2013).

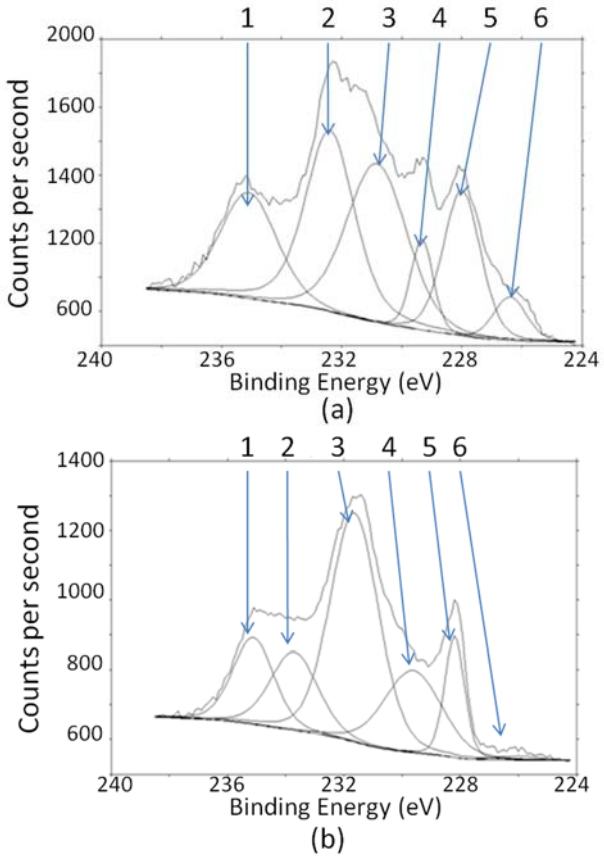

Figure 20. Mo3d spectral line for (a) MBT5 and (b) MBT20.

On the other hand, the CBT show only metallic Cu2p peaks at 232 and 252 eV for the 3/2 and 1/2 spins respectively (see Fig. 21)(Espinós et al. 2002). (Note: There is a small peak at 945 eV in both Cu spectra. This is a Cu3p3/2 satellite peak (Parmigiani et al. 1992).) This also shows that there is no bonding between Cu and F.

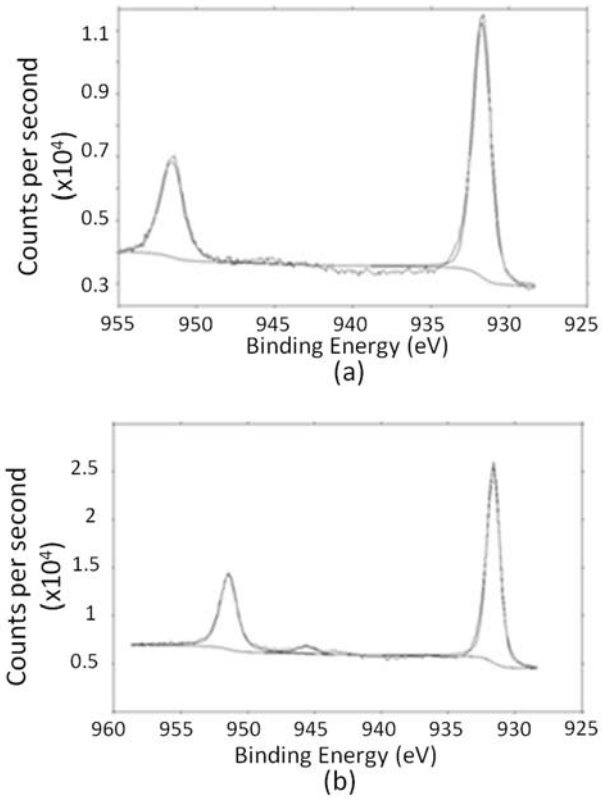

Figure 21. Cu2p spectral line for (a) CBT5 and (b) CBT20.

Also, due to the presence of the Cu3s peaks, tight scans of the strong Al2p peak were not used because they fall in the same binding energy range,(Herrera-Fierro 1993) instead Al2s was analyzed. There is still a Cu3s peak in the same region, but because there is only one peak from Cu, and the binding energies are spaced well enough to see 2 distinct peaks, Al2s was the better candidate for peak identification. For CBT samples, the Al2s peak was comprised of Al-O (119 eV) and Al-F (121 eV) binding energies.(see Fig. 22c and 22d)(Hess et al. 1993). It is noted that the peak located at 122 eV in the CBT5 and CBT20 Al spectra is the Cu3s peak(Parmigiani et al. 1992). The Al2s peak was used for both CBT samples

and Al2p was used for the MBT samples. The Al2p line showed Al-O bonds at ~74.0 eV and Al-F at 75.2 eV (Fig. 22a and 22b). Figure 22e shows the ratio of Al-F peak intensity to Al-O peak intensity for each sample.

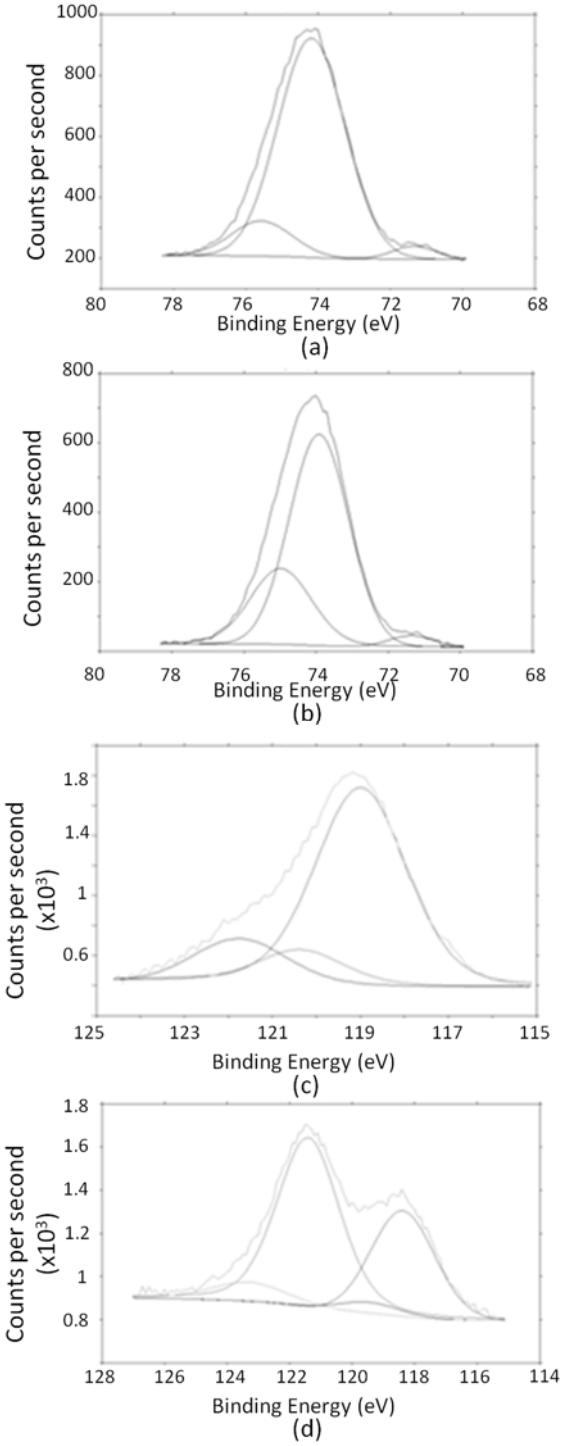
Counts per second
1000
800
600
400
200
80
78
76
74
72
70
68
Binding Energy (eV)
(a)
Counts per second
800
600
400
200
80
78
76
74
72
70
68
Binding Energy (eV)
(b)
Counts per second
(x10³)
1.8
1.4
1
0.6
125
123
121
119
117
115
Binding Energy (eV)
(c)
Counts per second
(x10³)
1.8
1.6
1.4
1.2
1
0.8
128
126
124
122
120
118
116
114
Binding Energy (eV)
(d)

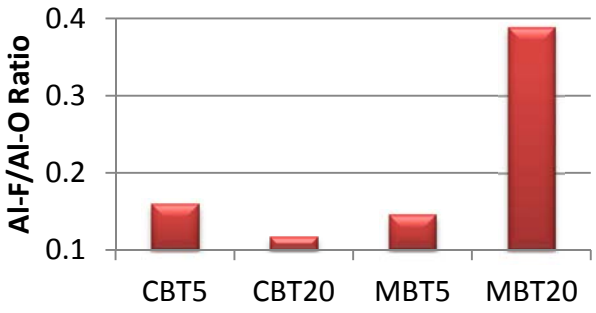

(e)

Figure 22. Al2p spectra for (a) MBT5 and (b) MBT20 and Al2s spectra for (c) CBT5 and (d) CBT20 and (e) graphical representation of Al-F bonds to Al-O bonds present in each sample.

Although Al-F bonds are detected in all samples, the MBT samples show an increase in the ratio of Al-F/Al-O bonding while the CBT samples show a decrease. The increase in Al-F bonding was expected with increasing PFPE loading, but the CBT samples showed a decline. This decline along with the decreasing HF gas signal from CBT5 to CBT20 provides new information about the location of the fluorine.

In addition to Al-F bonds present in CBT samples the F1s line shows an additional peak at 688 eV(Herrera-Fierro 1993) for CBT5 and 690 eV(J. M. Lee et al. 2009) in the CBT20 sample (see Fig. 23c and 23d). These peaks are both indicative of C-F bonds and were only distinguished in the CBT samples. The MBT samples only show one fluorine peak at 686 eV (Fig. 23a and 23b).

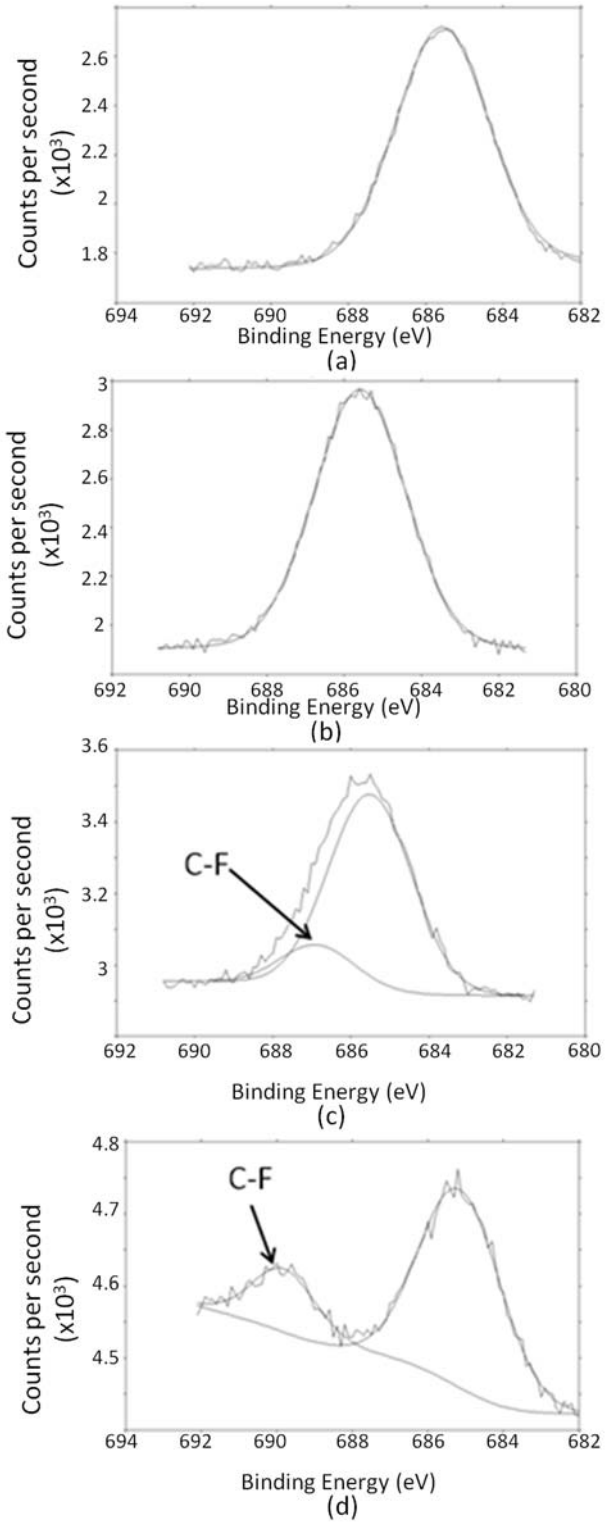

Figure 23. F1s spectra for (a) MBT5, (b) MBT20, (c) CBT5 and (d) CBT20.

This along with the increase in HF gas production suggests that the Al-MoO_3 blends catalyze the decomposition of PFPE while the Al-CuO blends do not. This is seen in the F1s spectra for CBT versus MBT. The improved decomposition of PFPE in the MBT samples along with the increasing formation of Al-F bonds confirm that the low temperature surface chemistry shown by the PIR increases flame speed in these samples.

Conclusion

Combustion characterization analyses using high speed imaging, XPS, QMS, and DSC were performed for varying concentrations of PFPE in Al/MoO_3 and Al/CuO composites in order to examine the influence of fluorine surface chemistry on reactivity. Results show that the performance of the thermite-PFPE blends is highly dependent on the oxidizing agent. The PFPE blends with MoO_3 show an increase in reactivity while the blends with CuO show a decrease in reactivity when increasing PFPE concentration. We observed a decline in formation of AlF_3 in CBT samples but an increase in AlF_3 formation in the MBT samples. The potential surface chemistry between Al_2O_3 and F from PFPE is negated by competitive Al-O, but thermodynamically favorable formation from CuO with lower bond dissociation energy than F or the CF_2 radical. When using an oxidizer with a BDE similar to that of the C-C or C-F bond (i.e. MoO_3), PFPE can

promote reactivity via catalytic behavior of the alumina shell to help decompose PFPE more efficiently and improve the low temperature surface chemistry and overall reactivity.

CHAPTER IV: Improving Aluminum Particle Reactivity by Annealing and Quenching Treatments: Synchrotron X-ray Diffraction Analysis of Strain

Abstract

In bulk material processing, annealing and quenching metals such as aluminum (Al) can relieve residual stress and improve mechanical properties. On a single particle level, affecting mechanical properties may also affect Al particle reactivity. This study examines the effect of annealing and quenching on the strain of Al particles and the corresponding reactivity of aluminum and copper oxide (CuO) composites. Micron-sized Al particles were annealed and quenched according to treatments designed to affect Al mechanical properties. Synchrotron X-ray diffraction (XRD) analysis of the particles reveals the thermal treatment increased the dilatational strain of the aluminum-core, alumina-shell particles. Flame propagation experiments also show thermal treatments effect reactivity when combined with CuO. An effective annealing/quenching treatment for increasing aluminum reactivity was identified. These results show that altering the mechanical properties of Al particles affects their reactivity.

Introduction

Composite energetic materials consist of a metallic fuel (i.e., aluminum (Al)) and a metal oxide (i.e., copper oxide (CuO)). These composites are widely studied due to their high energy densities and heats of combustion. A main goal of much published research studying aluminum combustion is to understand and improve particle reactivity. Towards this end, many have proposed new Al synthesis strategies: such as altering the native aluminum oxide (Al2O3) coating with another passivating agent such as alkenes(Chung et al. 2009) or applying self-assembled monolayers (SAM) to the particle surface(K. S. Kappagantula, Pantoya, and Horn 2013). Various explanations for Al oxidation mechanisms have also been proposed, each strongly tied to the ignition mechanism and heating rate(Levitas et al. 2006; Levitas et al. 2007; M. A. Trunov, Schooenitz, and Dreizin 2006; Dreizin 1999; M. a Trunov et al. 2006; K.T. Sullivan et al. 2012; Rai et al. 2006; K. Sullivan and Zachariah 2010; Chakraborty and Zachariah 2014). All theories share a common theme for mass transport of fuel and oxidizer, but differ in how that diffusion is achieved (i.e., via (a) dispersion(Levitas et al. 2006; Levitas et al. 2007), (b) phase changes in the polymorphous passivation shell(M. A. Trunov, Schooenitz, and Dreizin 2006; Dreizin 1999; M. a Trunov et al. 2006) , (c) reactive sintering(K.T. Sullivan et al. 2012), (d) pressure gradient driven

processes(Rai et al. 2006; K. Sullivan and Zachariah 2010), and (e) induced electric field influences(Chakraborty and Zachariah 2014)). This article will not directly deal with any particular reaction mechanism, but rather investigate the influence of a new parameter, mechanical strain, which has only recently been considered in the study of Al oxidation(Levitas et al. 2006; Levitas et al. 2007; Levitas, Mccollum, and Pantoya 2015; Dikici, Pantoya, and Levitas 2010).

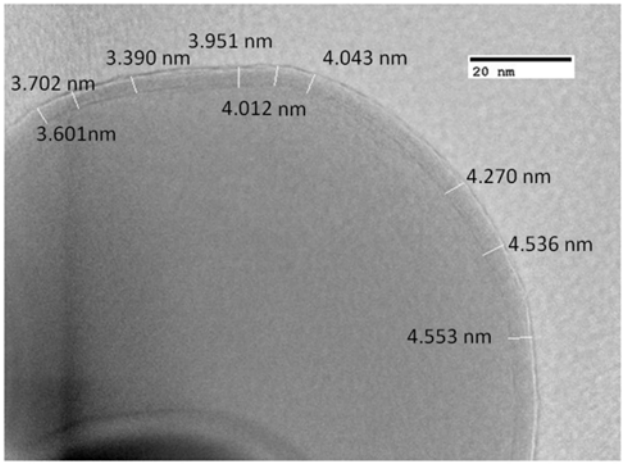

Figure 24. Transmission electron spectroscopy (TEM) image of a nano-scale Al particle to show alumina shell thickness. The average thickness is 4.01 nm. This thickness was used in the purity calculations for micron-scale Al particles (< 1% by mass oxide).

A typical aluminum particle consists of an aluminum core passivated by an alumina shell as seen in Fig. 24. Residual stress within an aluminum particle is induced during production. These are thermally induced stresses that are generated during the cooling stage. Stress builds in two stages during particle

synthesis: (1) within the aluminum core during cooling and prior to oxide shell formation; and, (2) during alumina shell formation until the core-shell system reaches ambient temperature conditions.

Within the molten aluminum droplet absent of a shell, stress develops as the molten aluminum droplet cools, because external surface layers start to shrink while the core is still hot and free to contract but its contraction is constrained by the external layers that have solidified and become rigid. In this way, the stress distribution in a naked aluminum particle is tensile in the core and compressive at the surface. Smaller particles cool at faster rates(Zheng et al. 2009a; Zheng et al. 2009b; Ozbilen, Unal, and Sheppard 2000) and should manifest larger internal stresses during production.

The shell is formed when oxygen is introduced at temperatures below the melting temperature of aluminum (i.e., < 660 °C(Hatch 1984)) and no higher than 440 °C (i.e., the phase transition of amorphous to gamma alumina(Dorre and Hubner 2011)). At this point, another residual stress develops because there exists a mismatch of thermal expansion coefficients (i.e., a, linear coefficient; or, b, volumetric coefficient) between the newly formed alumina shell (i.e., a_{ox} =5 x 10^{-6} K^{-1} and box= 8 x 10^{-6} K^{-1}(Dorre and Hubner 2011)) and aluminum core (a_m = 23 x 10^{-6} K^{-1} and b_m = 69 x 10^{-6} K^{-1} (Hatch 1984)). Cooling from 440 °C to ambient

will induce shrinkage in the core while the shell remains relatively rigid, i.e., there is an order of magnitude difference in expansion coefficients. The internal radius of the oxide sphere is forced to decrease and stresses arise at the interface of the core-shell.

Isothermal stress relief is a common approach to stress relaxation(Throop, Underwood, and Legar 1971; James 1987; L. W. Crane 1979). This technique involves the uniform heating of a material to a specified temperature below the melting temperature, holding at that temperature for a period of time, followed by cooling to control the re-introduction of desirable thermal stresses. This sequence of steps is referred to as annealing followed by quenching. Timoshenko and others(Throop, Underwood, and Legar 1971; James 1987; L. W. Crane 1979; Vilms and Kerps 1982; Kingery 1955) explain significant microstructural changes take place that promote stress relief at about two-thirds the temperature at which the stresses were formed. In the case of Al particles, the amorphous alumina shell is formed at roughly 440 °C such that annealing temperatures should at least be 293 °C. Interestingly, Firmansyah et al. examined the stress state of nano-aluminum powder upon continuous heating using a high temperature XRD and found that Al particles experience a zero-stress state at 300 °C(Firmansyah et al. 2012).

The main mechanism that causes relaxation of locked-in stresses for annealing temperatures < 400°C is classical diffusional creep. This mechanism enables counterbalancing regions of tensile and compressive stresses to contract or expand slightly, and thus to redistribute. This is also a time dependent process and determining the optimum temperature and duration for annealing and quenching has not previously been investigated for aluminum particles. Some experimental work on other metals has revealed a relevant conclusion: while the annealing time is important, creep is a logarithmic process such that most relief is obtained at a given temperature rapidly(James 1987). Data presented by Adeyemi et al. for carbon steel suggests annealing times on the order of 10 minutes should be sufficient to relieve stress(Adeyemi, Modlen, and Stark 1983). Even for the annealing temperature of 500oC, 80% of the residual stress is relieved in 5 minutes. Bulk aluminum alloys have been studied for creep behavior (Prasad, Sastry, and Vasu 1970). Prasad et al. studied creep at 87 and 200 °C and found the effects of stress increments and decrements to be different(Prasad, Sastry, and Vasu 1970). This is an important finding because it implies stress variations are significant in the temperature ranges we are most interested (i.e., < 400 °C).

Quenching is another important variable to consider. Evancho et al. showed that slow cooling may re-introduce thermal stresses that are undesirable (e.g., like the residual stress) and lead to lower strength(Evancho and Staley 1974). Faster cooling rates may effectively 'freeze' the stress state such that purposefully induced desirable thermal stress do not have time to relax, leading to higher strength. The hypothesis is: faster cooling rates will produce aluminum particles with optimal mechanical properties promoting optimal reactivity.

Dikici et al. showed preliminary evidence that annealing and quenching Al particles affects reactivity (Dikici, Pantoya, and Levitas 2010). They heated Al particles to a prescribed temperature then cooled them to room temperature and found that some thermal treatments lead to improved flame speeds. Their powders were allowed to cool at two different rates. The samples that were cooled at 0.06 KPS (Kelvin per second) showed flame speeds comparable to the untreated samples, but when the cooling rate was raised to 0.13 KPS, the flame speeds for micron scale Al and molybdenum trioxide (MoO3) improved for one case and worsened for the other. More recently, Levitas et al. extended the work by Dikici et al. by focusing on micron scale Al particles and using a different metal oxide (i.e., copper oxide (CuO))(Levitas, Mccollum, and Pantoya 2015). They examined flame speeds and showed certain thermal treatments were consistent

with predictions of the melt dispersion mechanism, effectively expanding the realm of this reaction mechanism towards optimization of micron scale Al particles (Levitas, Mccollum, and Pantoya 2015).

The objective of this study is to fundamentally quantify changes in strain associated with Al particle thermal treatments and examine energy propagation behavior of treated Al particles combined with CuO. These extensions enable an understanding of how thermal treatment and mechanical properties couple to influence the reactivity of Al particles with a solid oxidizer. Improving Al reactivity with a relatively simplistic heat treatment approach may greatly improve their functional application.

Experimental

Sample Preparation

Aluminum particles were procured from Alfa Aesar (Ward Hill, MA). Their average diameter was determined using an AccuSizer 780 optical particle size analyzer (Santa Barbara, CA). The Al particles were suspended in filtered water (specifically, 2 mg Al/80 ml water) and sonicated for 60 minutes in cycles of 10 seconds on, 10 seconds off in order to avoid heating. The sample was then pulled via a syringe pump for analysis. Particle length (diameter) is calculated and

plotted as a count-based measurement. The plot for the untreated Al is shown in Fig. 25a and the size data is given in Fig. 25e. The oxide thickness used for purity calculations was estimated at 4 nm (i.e., >1% oxide concentration, see Fig. 24). The untreated Al particles have an average diameter of 5 microns.

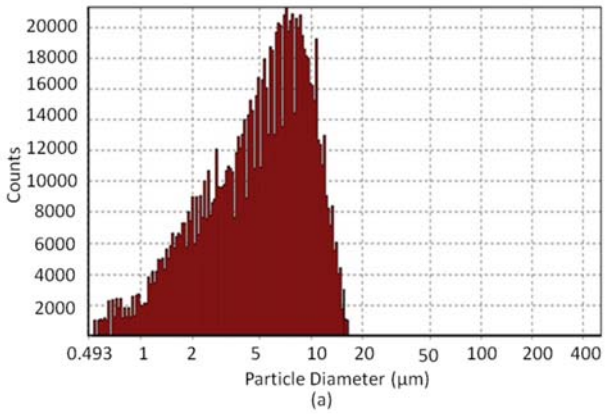
Counts
20000
18000
16000
14000
12000
10000
8000
6000
4000
2000
0.493 1 2 5 10 20 50 100 200 400
Particle Diameter (µm)
(a)

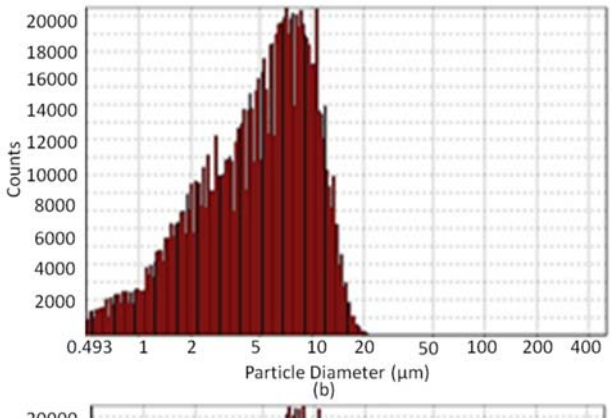
Counts
20000
18000
16000
14000
12000
10000
8000
6000
4000
2000
0.493 1 2 5 10 20 50 100 200 400
Particle Diameter (µm)
(b)

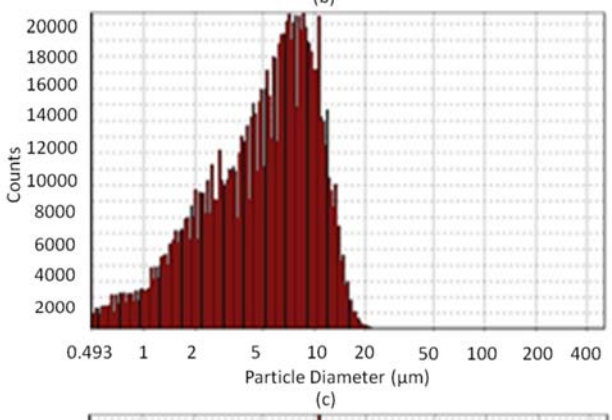
Counts
20000
18000
16000
14000
12000
10000
8000
6000
4000
2000
0.493 1 2 5 10 20 50 100 200 400
Particle Diameter (µm)
(c)

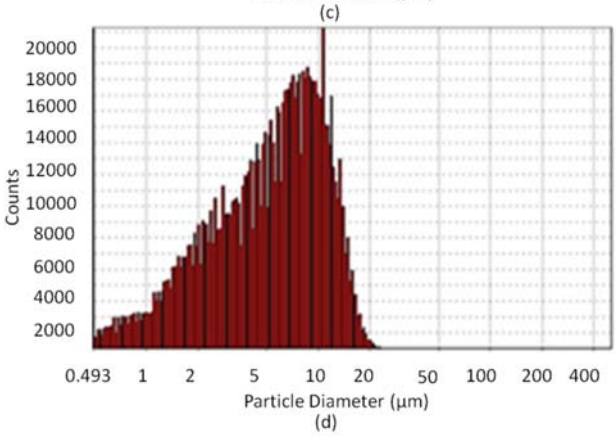
Counts
20000
18000
16000
14000
12000
10000
8000
6000
4000
2000
0.493 1 2 5 10 20 50 100 200 400
Particle Diameter (µm)
(d)

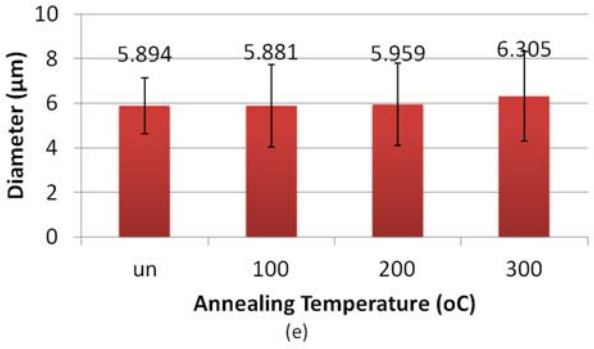

Figure 25. Particle size distribution of (a) untreated Al and Al annealed to (b) 100 °C, (c) 200 °C, (d) 300 °C and (e) average particle diameter with standard deviation for each Al powder sample.

Because the oxide layer thickness is independent of Al particle size, the oxide thickness used for purity calculations was estimated at 4 nm (i.e., >1% oxide concentration(see Fig. 24)). The untreated Al particles had an average diameter of 5.9 microns.

Aluminum particles (200 mg) were loaded into ceramic trays and subjected to various annealing temperatures and quenched to room temperature. This process used a Neytech Qex vacuum oven (Torrance, CA). This is a programmable oven, such that the powder was annealed to 100, 200 or 300°C at a controlled rate of 10 KPM, held at the prescribed temperature for 15 minutes then removed from the oven and quenched via refrigeration to room

temperature in air at standard pressure. Powder temperature was monitored using an InstruNet Direct to Sensor system (Charlestown, MA) and Type K thermocouples from Omega Engineering (Stamford, CT). Aluminum temperature was monitored for each thermal cycle and Fig. 26 shows the temperature response as a function of time.

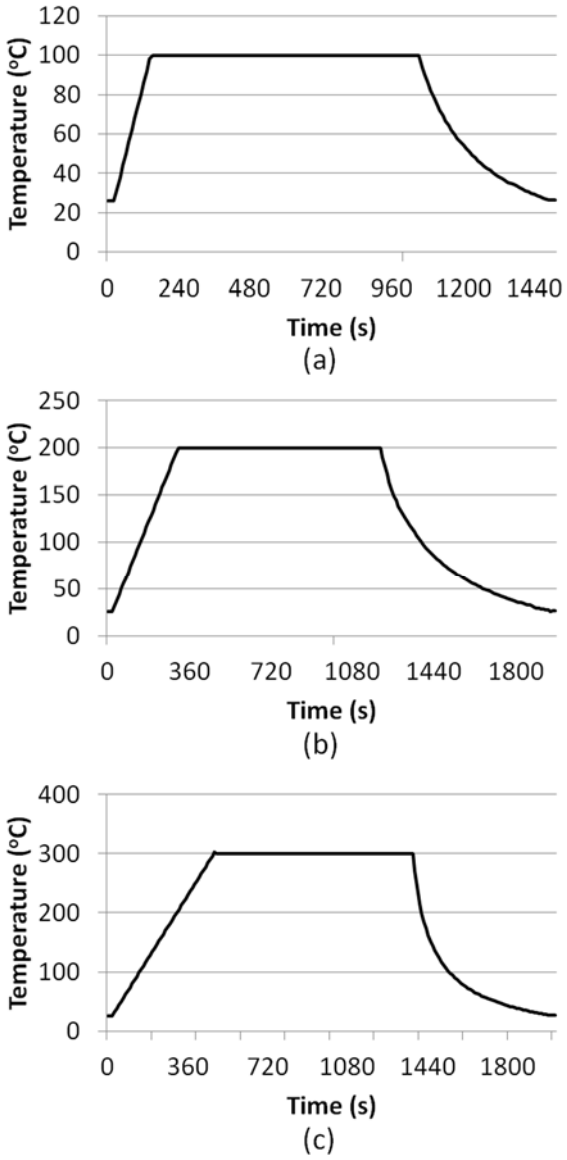

Figure 26. Temperature plots for Al thermal cycles to (a) 100 °C, (b) 200 °C and (c) 300 °C.

For the natural convection conditions that exist in these experiments, materials cool according to a lump capacitance model. The quenching rate is an exponential function of time as shown in Eq. (16). The temperature evolution reduces exponentially and experimental results are approximated by Eq. (16).

$$T = T_a + (T_0 - T_a) \exp(-At) \text{ with } A = 0.0078\ s^{-1} \quad (16)$$

In Eq. (17) T_a is ambient temperature, T_0 is annealing temperature, t is time and A is determined by examining the exponential plots of the cooling curves and identifying the coefficient. An average quenching rate ranges from 0.13 to 0.38 Kelvin per second (KPS) depending on annealing temperature.

The Al particles were then mixed with 50 nm average particle diameter spherical CuO particles (Sigma Aldrich (St. Louis, MO)) to an equivalence ratio of 1.2 (i.e., slightly fuel rich). The mixing process is well documented(C. a. Crane, Pantoya, and Weeks 2014; Feng et al. 2013; K. Kappagantula, Crane, and Pantoya 2014) but will be summarized here. The dry powders were weighed and suspended in hexane and mixed using a Misonix Sonicator 3000 probe for 2 minutes. The solution is poured into a Pyrex dish and hexane evaporated in a fume hood for 24 hours. The dry powders were retrieved and sieved to break up large agglomerations.

The powder is carefully loaded into 3 mm inner diameter, 8 mm outer diameter, 10 cm long quartz tubes containing 850 mg of powder each. The theoretical maximum density (TMD) of the loose powder is determined by a weighted average of the bulk densities of Al (2.7 g/cm^3), Al_2O_3 (3.95 g/cm^3), and

CuO (6.31 g/cm^3). This is calculated using Eq. (17) where *M* is the percent mass of reactant *i* and *ρ* is the density for each reactant.

$$\mathbf{TMD} = \frac{\mathbf{1}}{\sum_{\mathbf{i}} \mathbf{M_i} \frac{\mathbf{1}}{\boldsymbol{\rho}_{\mathbf{i}}}} \qquad (17)$$

The calculated TMD is 5.46 g/cm^3 and the bulk density is 1.04 g/cm^3 such that tubes were loaded to 19% TMD.

Strain Measurements

X-Ray Diffraction experiments were performed at the Advanced Light Source on beamline 12.3.2 using a micron focused synchrotron x-ray beam. This is a unique facility that allows measurement of micron-scale samples. Aluminum powder samples were spread over glass slides and scanned under the x-ray beam (either polychromatic or monochromatic) while a diffraction pattern was collected at each step using a DECTRIS Pilatus 1 M detector. The measured relative small shifts in the reflection positions in the Laue pattern provides the deviatoric strain tensor of the material while the measurement of the energy of one reflection provides the dilatational component. Data were processed using XMAS software(Kunz et al. 2009). The beamline experimental setup and capabilities have been described elsewhere(Tamura 2013).

Flame Speed Measurements

Figure 27 illustrates a typical powder filled tube arrangement for measuring flame speed and the apparatus is described in more detail elsewhere(Dikici, Pantoya, and Levitas 2010) but is summarized here.

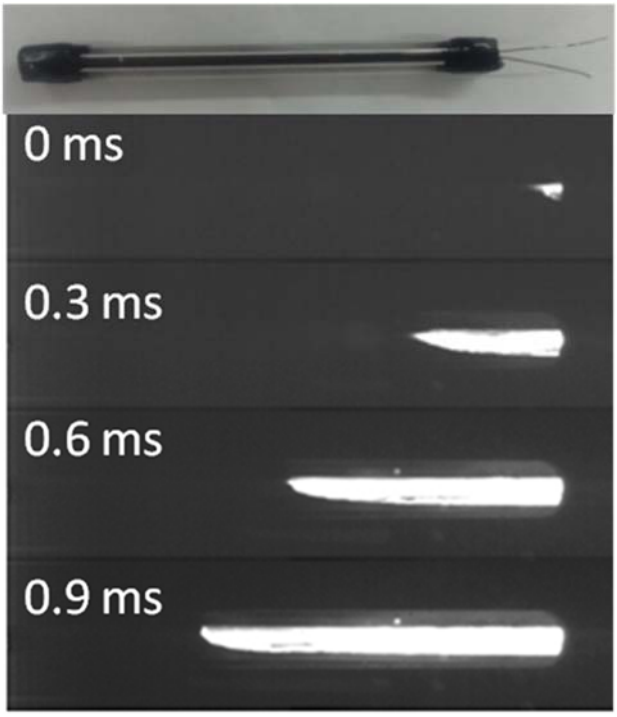

Figure 27. Powder filled quartz tube and representative still frame images time stamped of powder filled quartz tube and flame propagation. Bulk density is 19% theoretical maximum density. Note nichrome wire extruding for left end of the tube.

Both ends of the tube were sealed with one side securing a length of nickel-chromium wire for ignition. Five experiments per annealing temperature were performed to establish repeatability. Each tube was placed inside a blast chamber for ignition and flame propagation experiments. The powders were ignited and flame propagation was observed through a viewing window in the chamber (as seen in Fig. 28). The reaction was recorded with a Phantom v7 (Vision Research, Wayne, NJ) high speed camera at a rate of 29,000 frames per second and 512 x 128 resolution. The camera was aligned perpendicular to the direction of flame propagation. Flame speed was determined by tracking the flame front through a referenced time and distance using the Vision Research Software. The resolution of the flame speed for this diagnostic is 0.1 m/s. The largest source of uncertainty in the measurement is due to repeatability and is shown for each data set in the results.

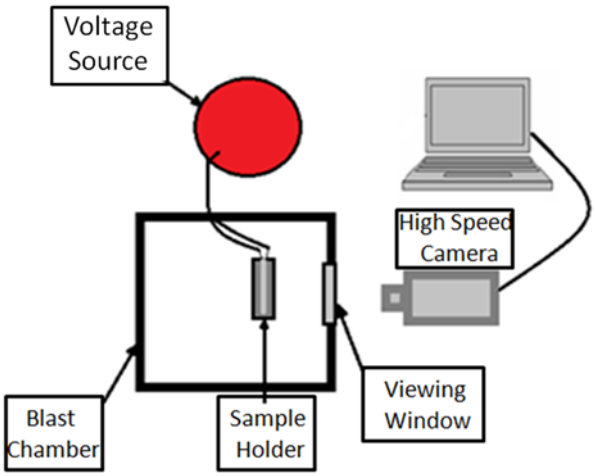

Figure 28. Ignition setup for tracking energy propagation.

Results

Further particle size analyses were performed for each Al sample after thermal treatment. Figures 25b-d show the plots for Al particle sizing and the average particle diameter and distribution is given in Fig. 25e. This data shows that the thermal treatments did not result in any sintering or agglomerations and that the average diameter is consistent (about 5.9 µm).

Figure 29 shows results of dilatational strain (i.e. change in volume) distribution measurements of aluminum particles that were (a) untreated and annealing to (b) 100°C, (c) 200°C and (d) annealed to 300°C. Table 6 presents the count based averages for dilatational strain for each annealing temperature. The average strain for the samples annealed to 100 and 200 °C fall within the resolution of the machine ($2x10^{-5}$), so their percent increase was negligible.

However, the aluminum particles annealed to 300°C and cooled to room temperature showed a significant dilatational strain increase from the baseline Al particles (i.e. 660%). It is noted that these measurements are of the aluminum core because the alumina shell is too thin (i.e., less than 5 nm) to resolve volume based strain measurements using this approach.

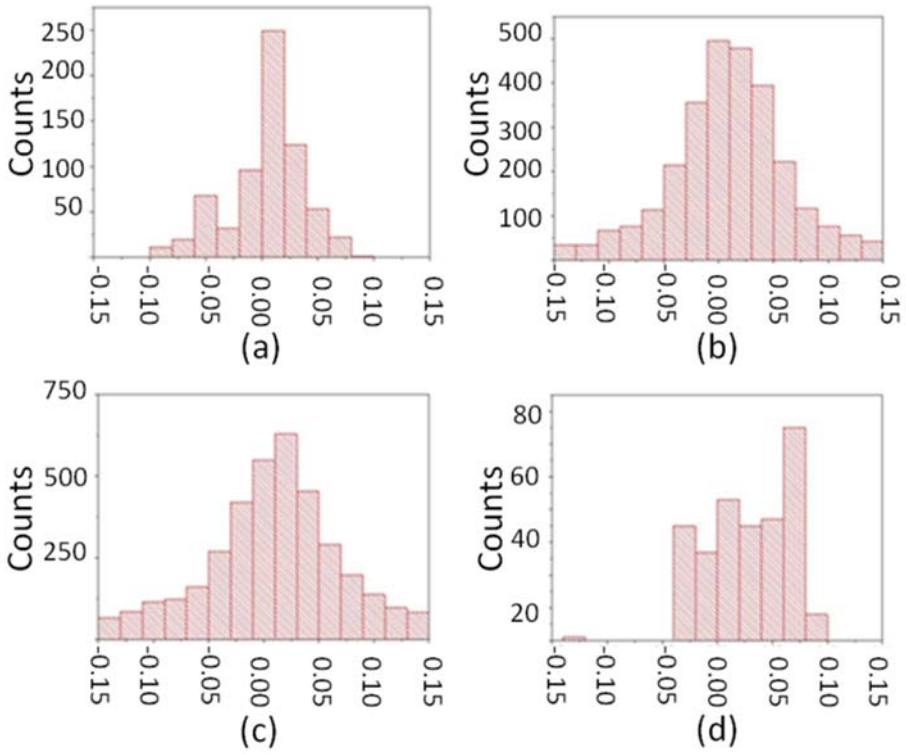

Figure 29. Dilatation strain for (a) untreated particles and particles annealed to (b) 100 °C, (c) 200 °C and (d) 300 °C.

Figure 30 shows flame speed as a function of annealing temperature. The samples annealed to 100°C experience a 2% increase in flame speed from the baseline; and, when annealed to 200°C flame speed increases by 3%. Once the

samples are annealed to 300°C, they experience a 23% increase in flame speed. This is a significant increase in reactivity for the composite annealed to 300°C but not for the other annealing temperatures. These results are also summarized in Table 6.

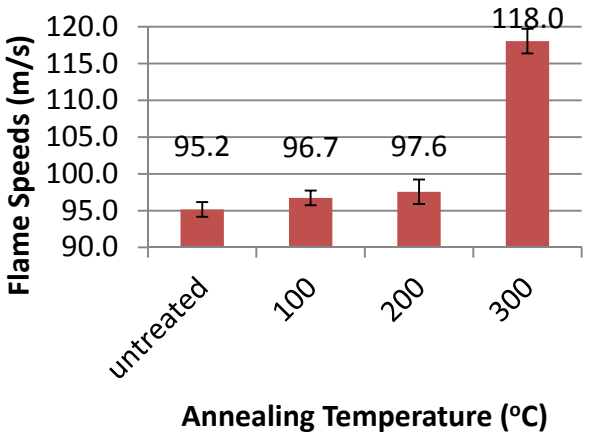

Figure 30. Flame speed as a function of annealing temperature. Average values for flame speed are reported above the bar and standard deviation in the measurements is also shown.

Table 6. Dilatational strain in Al particles, flame speeds when combined with CuO, and percent increase for all Al annealing temperatures. The average strain for the samples annealed to 100 and 200 °C fall within the resolution of the machine, so their percent increase was negligible.

Annealing Temperature (°C)	Average strain	% increase	Flame Speed (m/s)	% increase
untreated	1.00E-05	---	95.2	---
100	1.47E-05	---	96.7	---
200	1.53E-05	---	97.6	---
300	3.25E-05	660	118	24

Discussion

Figure 29 shows that compared to the baseline, volumetric strain increases as annealing temperature increases. According to Fig. 29 and Table 6, average dilatational strain increases by 660% after thermal treatment to 300 ^{o}C but is unchanged in the samples annealed to 100 and 200 ^{o}C. Diffusional creep resistance occurs in samples when the annealing temperature is below a critical fraction of the melt temperature (i.e., T_m= 660 ^{o}C for Al)(Kitagawa, Jaske, and Morrow 1969). Kitagawa et al. investigated creep response in bulk Al samples subjected to a variety of temperatures (i.e., from $0.32T_m$ (~27 ^{o}C) to $0.55T_m$ (~240 ^{o}C)) for different number of thermal treatment cycles. They were interested to see the Average creep rate for each temperature over a variety of thermal cycles and found that the transition temperature for Al to exhibit creep acceleration is $0.4T_m$ (i.e., 100 ^{o}C) and the maximum acceleration of creep for Al occurs at about $0.52T_m$ (212 ^{o}C). Figure 29 shows that the samples annealed to 100 and 200^{o}C show little response in terms of dilatational strain, consistent with annealing temperatures below the critical temperature for maximum acceleration of creep (i.e., 212 ^{o}C). However, once this critical temperature is passed (i.e., 300 ^{o}C), the Al particles responded with a 660% increase in dilatational strain. The effect of this trend is seen in the flame speed results. The Al samples annealed to 100 and

200 ^{o}C showed little change from the untreated case, but for the 300 ^{o}C case, flame speeds increased by 24%.

Ultimately, the annealing and quenching treatment effectively increased the overall strain. It is important to note that at higher annealing temperature or longer annealing times, particles could experience shell growth and/or oxide phase change. Amorphous alumina begins to transition to gamma-phase alumina around 440 ^{o}C, such that annealing beyond this temperature would affect the shell microstructure, which may also impact reactivity. Also, annealing to temperatures past 440 ^{o}C for an extended time (60+ minutes) would result in oxide layer growth as shown by Gesner et al.(Gesner, Pantoya, and Levitas 2012). They annealed 95 nm diameter Al particles to 480 ^{o}C for a variety of hold times and saw an increase in oxide shell thickness from 2.7 to 8.3 nm when held for 150 minutes but negligible shell growth for times applied in this study (and in this study annealing temperatures did not exceed 300 °C).

Thermal treatment is purposefully designed to relax residual stresses by annealing then reintroduce desirable stresses by quenching. While thermal treatments are relatively established for bulk metal processing, manipulation of mechanical properties for particles that consist of a core-shell structure are not well understood. In this study, results for thermal treatment of particles appear

to be consistent with theory for bulk metals. The benefit of thermal treatment from Fig. 29 and 30 is that the annealed and quenched Al powders now have experience higher strain that also increases macroscopic energy propagation.

Conclusion

This study examines the effect of aluminum powder annealing and quenching treatments on the strain in of aluminum particles and corresponding reactivity. Micron-sized aluminum was annealed and quenched according to treatments designed to affect mechanical properties. Synchrotron x-ray diffraction (XRD) analysis of the particles reveals annealing increased the dilatational strain of the Al particles. Diffusional creep is the primary mechanism affecting strain and for powder annealed to 300 ^{o}C, a 660% increase in dilatational strain was observed. However, annealing to 100 or 200 ^{o}C showed no significant increase in dilatational strain. Treated Al powder was then mixed with CuO to assess reactivity. Flame speed measurements similarly show the 300°C annealed sample produces the highest flame speed. These results reveal that altering the mechanical properties of aluminum particles affects their reactivity, particularly when combined with a solid oxidizer.

OVERVIEW

Chapter two investigates the combustion performance of various Al particle sizes coated with PFPE (a liquid fluorinated oligomer). Flame speeds, differential scanning calorimetry (DSC), thermogravimetric analysis (TGA) and quadruple mass spectrometry (QMS) were performed for Al- PFPE blends with varying Al particle sizes (80, 100, 120 and 5500 nm in average diameter). The results show that the combustion performance of these blends is highly dependent on the Al_2O_3 concentration and exposed surface area. There is a balance to optimizing Al particle reactivity between activating Al particles with exothermic surface chemistry versus the unreacted alumina that contributes a thermal heat sink during energy generation. Overall, flame speed is inversely proportional to the apparent activation energy for the blend, with lower activation energy correlating with higher flame speeds. Also, combustion performance is optimized when the material concentrations are balanced such that they burn in a conductively driven manner.

Once fundamental combustion was understood for Al-PFPE blends, chapter three covered combustion characterization analyses for varying concentrations of PFPE in Al/MoO_3 and Al/CuO composites in order to examine the influence of fluorine surface chemistry on reactivity using high speed imaging,

XPS, QMS, and DSC. Results show that the performance of the thermite-PFPE blends is highly dependent on the metal oxide. The PFPE blends with MoO_3 show an increase in reactivity while the blends with CuO show a decrease in reactivity when increasing PFPE concentration. We observed a decline in formation of AlF_3 in CBT samples but an increase in AlF_3 formation in the MBT samples. The potential surface chemistry between Al_2O_3 and F from PFPE is negated by competitive Al-O, but thermodynamically favorable formation from CuO with lower bond dissociation energy than F or the CF_2 radical. When using an oxidizer with a BDE similar to that of the C-C or C-F bond (i.e. MoO_3), PFPE can promote reactivity via catalytic behavior of the alumina shell to help decompose PFPE more efficiently and improve the low temperature surface chemistry and overall reactivity.

Chapter four examines the effect of aluminum powder annealing and quenching treatments on the strain in of aluminum particles and corresponding reactivity. Micron-sized aluminum was annealed and quenched according to treatments designed to affect mechanical properties. Synchrotron x-ray diffraction (XRD) analysis of the particles reveals annealing increased the dilatational strain of the Al particles. Diffusional creep is the primary mechanism affecting strain and for powder annealed to 300 ^{o}C, a 660% increase in

dilatational strain was observed. However, annealing to 100 or 200 ^{o}C showed no significant increase in dilatational strain. Treated Al powder was then mixed with CuO to assess reactivity. Flame speed measurements similarly show the 300°C annealed sample produces the highest flame speed. These results reveal that altering the mechanical properties of aluminum particles affects their reactivity, particularly when combined with a solid oxidizer.

BIBLIOGRAPHY

Adeyemi, M.B., G.F. Modlen, and R.A. Stark. 1983. "Stress Relaxation in Cold Worked Mild Steel." *Metal Science* 17 (7): 43–47.

Al-Kandari, H., a.M. Mohamed, S. Al-Kandari, F. Al-Kharafi, G.a. Mekhemer, M.I. Zaki, and a. Katrib. 2013. "Spectroscopic Characterization–catalytic Activity Correlation of Molybdena Based Catalysts." *Journal of Molecular Catalysis A: Chemical* 368-369 (March). Elsevier B.V.: 1–8. doi:10.1016/j.molcata.2012.11.013.

Atkins, Peter, and Julio de Paula. 2010. *Physical Chemistry*. 9th ed. Oxford University Press.

Boswell, P.G. 1980. "On the Calculation of Activation Energies Using a Modified Kissinger Method." *Journal of Thermal Analysis and Calorimetry* 18 (353).

Cervantes, Octavio G., Joshua D. Kuntz, Alexander E. Gash, and Zuhair a. Munir. 2011. "Activation Energy of Tantalum–tungsten Oxide Thermite Reactions." *Combustion and Flame* 158 (1). The Combustion Institute.: 117–22. doi:10.1016/j.combustflame.2010.07.023.

Chakraborty, Purnendu, and Michael R. Zachariah. 2014. "Do Nanoenergetic Particles Remain Nano-Sized during Combustion?" *Combustion and Flame*

161 (5). The Combustion Institute.: 1408–16. doi:10.1016/j.combustflame.2013.10.017.

Chen, Y., F.V. Lawrence, C.P.L. Barkan, and J.A. Dantzig. 2006. “Heat Transfer Modelling of Rail Thermite Welding.” *Proc. Inst. Mech. Eng., Part F* 223 (3): 207–17.

Chung, S.W., E.A. Guliants, D.W. Bunker, C.E., Hammerstroem, W. Douglas, Y. Deng, M.A. Burgers, P.A. Jelliss, and S.W. Buckner. 2009. “Capping and Passivation of Aluminum Nanoparticles Using Alkyl-Substituted Epoxides.” *Langmuir : The ACS Journal of Surfaces and Colloids* 25 (16): 8883–87.

Chupas, P.J., and C.P. Grey. 2004. “Surface Modification of Fluorinated Aluminas: Application of Solid State NMR Spectroscopy to the Study of Acidity and Surface Structure.” *Journal of Catalysis*, 69–79.

Conner, Rusty W., and Dana D. Dlott. 2012. “Comparing Boron and Aluminum Nanoparticle Combustion in Teflon Using Ultrafast Emission Spectroscopy.” *The Journal of Physical Chemistry C* 116 (4): 2751–60. doi:10.1021/jp209912t.

Cottrell, T.L. 1958. *The Strengths of Chemical Bonds*. Butterworth, London.

Crane, C. a., M. L. Pantoya, and B. L. Weeks. 2014. “Investigating the Trade-Offs of Microwave Susceptors in Energetic Composites: Microwave Heating versus Combustion Performance.” *Journal of Applied Physics* 115 (10): 104106. doi:10.1063/1.4868337.

Crane, C., M. L. Pantoya, and Dunn. 2010. “Infrared Measurements of Energy Transfer from Energetic Materials to Steel Substrates.” *International Journal of Thermal Sciences* 49 (10): 1877–85.

Crane, Charles a., Michelle L. Pantoya, and Jerry Dunn. 2010. “Infrared Measurements of Energy Transfer from Energetic Materials to Steel Substrates.” *International Journal of Thermal Sciences* 49 (10). Elsevier Masson SAS: 1877–85. doi:10.1016/j.ijthermalsci.2010.06.005.

Crane, L.W. 1979. “Heat Treatment Methods Media.” *Inst. Metall. Tech.*, 1–10.

Deevi, S., V. Sikka, and C. Swindeman. 1997. “Application of Reaction Synthesis Principles to Thermal Spray Coatings.” *Journal of Materials Chemistry A* 32 (12): 3315–25.

Dikici, Birce, Michelle L. Pantoya, and Valery Levitas. 2010. “The Effect of Pre-Heating on Flame Propagation in Nanocomposite Thermites.” *Combustion and Flame* 157 (8): 1581–85. doi:10.1016/j.combustflame.2010.04.014.

Dorre, H., and H. Hubner. 2011. *Alumina: Processing, Properties and Applications*. Berlin: Springer.

Dreizin, Edward L. 1999. “On the Mechanism of Asymmetric Aluminum Particle Combustion.” *Combustion and Flame* 117 (4): 841–50.

Dyer, T.S., and Zuhair a. Munir. 1995. “The Synthesis of Nickel Aluminides by Multilayer Self-Propagating Combustion.” *Metall. Mater. Trans. B* 26 (603).

Espinós, J. P., J. Morales, a. Barranco, a. Caballero, J. P. Holgado, and a. R. González-Elipe. 2002. “Interface Effects for Cu, CuO, and Cu2O Deposited on SiO2 and ZrO2. XPS Determination of the Valence State of Copper in Cu/SiO2 and Cu/ZrO2 Catalysts.” *Journal of Physical Chemistry B* 106: 6921–29. doi:10.1021/jp014618m.

Evancho, J.W., and J.T. Staley. 1974. “Kinetics of Precipitation in Aluminum Alloys During Continuous Cooling.” *Metallurgical Transactions A* 5: 43–47.

Farley, Cory W, Michelle L Pantoya, Martin Losada, and Santanu Chaudhuri. 2013. “Linking Molecular Level Chemistry to Macroscopic Combustion Behavior for Nano-Energetic Materials with Halogen Containing Oxides.” *The Journal of Chemical Physics* 139 (7): 074701. doi:10.1063/1.4818167.

Feng, Jingyu, Guoqiang Jian, Qing Liu, and Michael R Zachariah. 2013. “Passivated Iodine Pentoxide Oxidizer for Potential Biocidal Nanoenergetic Applications.” *ACS Applied Materials & Interfaces* 5 (18): 8875–80. doi:10.1021/am4028263.

Firmansyah, Dudi Adi, Kyle Sullivan, Kwang-Sung Lee, Yong Ho Kim, Riyan Zahaf, Michael R. Zachariah, and Donggeun Lee. 2012. “Microstructural Behavior of the Alumina Shell and Aluminum Core Before and After Melting of Aluminum

Nanoparticles." *The Journal of Physical Chemistry C* 116 (1): 404–11. doi:10.1021/jp2095483.

Fischer, SH, and MC Grubelich. 1998. "Theoretical Energy Release of Thermites, Intermetallics, and Combustible Metals." In *International Pyrotechnics Seminar*.

Gesner, Jeffrey, Michelle L. Pantoya, and Valery I. Levitas. 2012. "Effect of Oxide Shell Growth on Nano-Aluminum Thermite Propagation Rates." *Combustion and Flame* 159 (11). The Combustion Institute.: 3448–53. doi:10.1016/j.combustflame.2012.06.002.

Hatch, J.E. 1984. *Aluminum: Properties and Physical Metallurgy*. Ohio.

Herrera-Fierro, Pilar. 1993. "Interfacial Chemistry of a Perfluoropolyether Lubricant Studied by X-Ray Photoelectron Spectroscopy and Temperature Desorption Spectroscopy." *Journal of Vacuum Science & Technology A: Vacuum, Surfaces, and Films* 11 (2): 354. doi:10.1116/1.578737.

Hess, A., E. Kemnitz, A. Lippitz, W.E.S. Unger, and D.H. Menz. 1993. "ESCA, XRD, and IR Characterization of Aluminum Oxide, Hydroxyfluoride, and Fluoride Surfaces in Correlation with Their Catalytic Activity in Heterogeneous Halogen Exchange Reactions." *Journal of Catalysis* 148: 270–80.

Hunt, Emily M., Steven Malcolm, Michelle L. Pantoya, and Freddie Davis. 2009. "Impact Ignition of Nano and Micron Composite Energetic Materials." *International Journal of Impact Engineering* 36 (6). Elsevier Ltd: 842–46. doi:10.1016/j.ijimpeng.2008.11.011.

Hunt, Emily M., and Michelle L. Pantoya. 2005. "Ignition Dynamics and Activation Energies of Metallic Thermites: From Nano- to Micron-Scale Particulate Composites." *Journal of Applied Physics* 98 (3): 034909. doi:10.1063/1.1990265.

Iordachescu, M., D. Iordachescu, E. Scutelnicu, J. Ruiz-Hervias, A. Valiente, and L. Caballero. 2010. "Influence of Heating Source Position and Dilution Rate in Achieving Overmatched Dissimilar Welded Joints." *Science Technology Welding and Joining* 15 (5): 378–85.

James, M R. 1987. “Relaxation of Residual Stresses: An Overview.” *Technology, Applications, Effects*.

Jian, Guoqiang, Nicholas W. Piekiel, and Michael R. Zachariah. 2012. “Time-Resolved Mass Spectrometry of Nano-Al and Nano-Al/CuO Thermite under Rapid Heating: A Mechanistic Study.” *The Journal of Physical Chemistry C* 116 (51): 26881–87. doi:10.1021/jp306717m.

Kappagantula, Keerti, Charles Crane, and Michelle Pantoya. 2013. “Determination of the Spatial Temperature Distribution from Combustion Products: A Diagnostic Study.” *The Review of Scientific Instruments* 84 (10): 104902. doi:10.1063/1.4822118.

———. 2014. “Factors Influencing Temperature Fields during Combustion Reactions.” *Propellants, Explosives, Pyrotechnics* 39 (3): 434–43. doi:10.1002/prep.201300154.

Kappagantula, Keerti, Michelle L. Pantoya, and Emily M. Hunt. 2012. “Impact Ignition of Aluminum-Teflon Based Energetic Materials Impregnated with Nano-Structured Carbon Additives.” *Journal of Applied Physics* 112 (2): 024902. doi:10.1063/1.4737118.

Kappagantula, Keerti S., Cory Farley, Michelle L. Pantoya, and Jillian Horn. 2012. “Tuning Energetic Material Reactivity Using Surface Functionalization of Aluminum Fuels.” *The Journal of Physical Chemistry C* 116 (46): 24469–75. doi:10.1021/jp308620t.

Kappagantula, Keerti S., Michelle L. Pantoya, and Jillian Horn. 2013. “Effect of Surface Coatings on Aluminum Fuel Particles toward Nanocomposite Combustion.” *Surface and Coatings Technology* 237 (December). Elsevier B.V.: 456–59. doi:10.1016/j.surfcoat.2013.08.035.

Karaman, M.E., D.A. Antelmi, and R.M. Pashley. 2001. “The Production of Stable Hydrophobic Surfaces by the Adsorption of Hydrocarbon and Fluorocarbon Carboxylic Acids onto Alumina Substrates.” *Colloids and Surfaces., A* 182: 285–98.

Kasai, Paul H., Wing T. Tang, and Patrick Wheeler. 1991. “Degradation of Perfluoropolyethers Catalyzed by Aluminum Oxide.” *Applied Surface Science* 51 (3-4): 201–11. doi:10.1016/0169-4332(91)90403-7.

Kingery, W.D. 1955. “Factors Affecting Thermal Stress Resistance of Ceramic Materials.” *Journal of the American Ceramic Society* 38 (1).

Kissinger, H.E. 1957. “Reaction Kinetics in Differential Thermal Analysis.” *Analytical Chemistry* 29 (1702).

Kitagawa, M., C.E. Jaske, and J. Morrow. 1969. “Influence of Temperature on Reversed Creed.” In *American Sociaty for Testing and Materials*, 100–110. San Fransisco, CA.

Knoezinger, H. 1978. “Catalytic Aluminas: Surface Models and Characterization of Surface Sites.” *Catalysis Reviews: Science and Engineering* 17 (1): 31–70.

Koch, Ernst-Christian. 2012. *Metal-Fluorocarbon Based Energetic Materials*. Wiley-VCH.

Kunz, M., N. Tamura, K. Chen, A.A. MacDowell, R.S. Celestre, M.M. Church, and E. Ustundag. 2009. “A Dedicated Superbend X-Ray Microdiffraction Beamline for Materials, Geo-, and Environmental Sciences at the Advanced Light Source.” *Review of Scientific Instruments* 80 (3): 035108.

Lee, Jeong Min, Sang Jin Kim, Ju Wan Kim, Phil Hyun Kang, Young Chang Nho, and Young Seak Lee. 2009. “A High Resolution XPS Study of Sidewall Functionalized MWCNTs by Fluorination.” *Journal of Industrial and Engineering Chemistry* 15: 66–71. doi:10.1016/j.jiec.2008.08.010.

Lee, M., K. Feng, X. Chen, N. Wu, A. Raman, J. Nightingale, E. Gawalt, D. Korakakis, Larry a Hornak, and A. Tiperman. 2007. “Adsorption and Desorption of Stearic Acid Self-Assembled Monolayers on Aluminum Oxide.” *Langmuir : The ACS Journal of Surfaces and Colloids* 23 (5): 2444–52.

Levitas, Valery I, Jena Mccollum, and Michelle L Pantoya. 2015. “Improving Micron - Scale Aluminum Core - Shell Particles Reactivity by Pre - Stressing.” *Scientific Reports*, no. Mdm: 1–12.

Levitas, Valery I., Blaine W. Asay, Steven F. Son, and Michelle Pantoya. 2006. "Melt Dispersion Mechanism for Fast Reaction of Nanothermites." *Applied Physics Letters* 89 (7): 071909. doi:10.1063/1.2335362.

———. 2007. "Mechanochemical Mechanism for Fast Reaction of Metastable Intermolecular Composites Based on Dispersion of Liquid Metal." *Journal of Applied Physics* 101 (8): 083524. doi:10.1063/1.2720182.

Levitas, Valery I., Birce Dikici, and Michelle L. Pantoya. 2011. "Toward Design of the Pre-Stressed Nano- and Microscale Aluminum Particles Covered by Oxide Shell." *Combustion and Flame* 158 (7). The Combustion Institute.: 1413–17. doi:10.1016/j.combustflame.2010.12.002.

Losada, Martin, and Santanu Chaudhuri. 2010. "Finite Size Effects on aluminum/Teflon Reaction Channels under Combustive Environment: A Rice-Ramsperger-Kassel-Marcus and Transition State Theory Study of Fluorination." *The Journal of Chemical Physics* 133 (13): 134305. doi:10.1063/1.3480020.

McCollum, Jena, Michelle L Pantoya, and Scott T. Iacono. 2015. "Activating Aluminum Particle Reactivity with Fluorine Oligomer Surface Coating." *Submitted to Journal of Physical Chemistry C*.

Miller, Hannah a., Bradley S. Kusel, Seth T. Danielson, James W. Neat, Eryn K. Avjian, Scott N. Pierson, Stephen M. Budy, David W. Ball, Scott T. Iacono, and Sharon C. Kettwich. 2013. "Metastable Nanostructured Metallized Fluoropolymer Composites for Energetics." *Journal of Materials Chemistry A* 1 (24): 7050. doi:10.1039/c3ta11603d.

Moore, David S., Steven F. Son, and Blaine W. Asay. 2004. "Time-Resolved Spectral Emission of Deflagrating Nano-Al and Nano-MoO3 Metastable Interstitial Composites." *Propellants, Explosives, Pyrotechnics* 29 (2): 106–11. doi:10.1002/prep.200400038.

Moore, J.J., and H.J. Feng. 1995. "Combustion Synthesis of Advanced Materials_ Part I. Reaction Parameters.pdf." *Progress in Materials Science* 39: 243–73.

Nixon, E P, M L Pantoya, D J Prentice, E D Steffler, M a Daniels, and S P D'Arche. 2010. "A Diagnostic for Quantifying Heat Flux from a Thermite Spray."

Measurement Science and Technology 21 (2): 025202. doi:10.1088/0957-0233/21/2/025202.

Oberg, K., P. Persson, A. Shchukarev, and B. Eliasson. 2001. “Comparison of Monolayer Films of Stearic Acid and Methyl Stearate on an Al2O3 Surface.” *Thin Solid Films* 397: 102–8.

Osborne, D., and Michelle Pantoya. 2007. “Effect of Aluminum Particle Size on the Thermal Degradation of Al/Teflon Mixtures.” *Combustion Science and Technology* 179 (8): 1467–80.

Ozawa, T. 1992. “Estimation of Activation Energy by Isoconversion Methods.” *Thermochimica Acta* 203 (159).

Ozbilen, S., A. Unal, and T. Sheppard. 2000. “Influence of Atomizing Gases on the Oxide-Film Morphology and Thickness of Aluminum Powders.” *Oxidation of Metals* 53: 1–22.

Pantoya, Michelle L, and Steven W Dean. 2009. “Thermochimica Acta The Influence of Alumina Passivation on Nano-Al / Teflon Reactions.” *Thermochimica Acta* 493: 109–10. doi:10.1016/j.tca.2009.03.018.

Pantoya, Michelle?L., and John?J. Granier. 2005. “Combustion Behavior of Highly Energetic Thermites: Nano versus Micron Composites.” *Propellants, Explosives, Pyrotechnics* 30 (1): 53–62. doi:10.1002/prep.200400085.

Parmigiani, F., G. Pacchioni, F. Illas, and P.S. Bagus. 1992. “Studies of the Cu□O Bond in Cupric Oxide by X-Ray Photoelectron Spectroscopy and Ab Initio Electronic Structure Models.” *Journal of Electron Spectroscopy and Related Phenomena* 59 (3): 255–69. doi:10.1016/0368-2048(92)87005-7.

Peri, J B. 1965. “A Model for the Surface of ? -Alumina ’.” *Journal of Physical Chemistry* 809 (8): 220–30.

Prasad, Y.V.R.K, D.H. Sastry, and K.I. Vasu. 1970. “A Study of Low Temperature Creep in Aluminum by Change in Stress Experiments: Thermal Activation of Attractive Junctions.” *Metal Science* 4 (69-73).

Puts, G.J., and P.L. Crouse. 2014. “The Influence of Inorganic Materials on the Pyrolysis of Polytetrafluoroethylene. Part 2: The Common Oxides of Al, Ga,

In, Zn, Cu, Ni, Co, Fe, Mn, Cr, V, Zr and La." *Journal of Fluorine Chemistry* 168 (December). Elsevier B.V.: 9–15. doi:10.1016/j.jfluchem.2014.08.012.

Rai, A., K. Park, L. Zhou, and M. R. Zachariah. 2006. "Understanding the Mechanism of Aluminum Nanoparticle Oxidation." *Combustion Theory and Modelling* 10 (5): 603–23.

Sanders, V. Eric, Blaine W. Asay, Timothy J. Foley, Bryce C. Tappan, Adam N. Pacheco, and Steven F. Son. 2014. "Reaction Propagation of Four Nanoscale Energetic Composites (Al/MoO3, Al/WO3, Al/CuO, and Bi2O3)." *Journal of Propulsion and Power* 23 (4). American Institute of Aeronautics and Astronautics: 707–14. Accessed July 29. http://cat.inist.fr/?aModele=afficheN&cpsidt=18938490.

Sarbak, Z. 1997. "Effect of Fluoride and Sodium Ions on Structural and Thermal Properties of Gamma-Al2O3." *Cryst. Res. Technology* 32 (4): 491–97.

Shigeta, M., and T. Watanabe. 2010. "Growth Model of Binary Alloy Nanopowders for Thermal Plasma Synthesis." *Journal of Applied Physics* 108 (4).

Sippel, Travis R., Steven F. Son, and Lori J. Groven. 2013. "Altering Reactivity of Aluminum with Selective Inclusion of Polytetrafluoroethylene through Mechanical Activation." *Propellants, Explosives, Pyrotechnics* 38 (2): 286–95. doi:10.1002/prep.201200102.

Sippel, Travis. R., Steven F. Son, and Lori J. Groven. 2013. "Modifying Aluminum Reactivity with Poly(Carbon Monofluoride) via Mechanical Activation." *Propellants, Explosives, Pyrotechnics* 38 (3): 321–26. doi:10.1002/prep.201200202.

Starink, M.J. 1996. "A New Method for the Derivation of Activation Energies from Experiments Performed at Constant Heating Rate." *Thermochimica Acta* 288 (97).

Sullivan, K, G Young, and M Zachariah. 2009. "Enhanced Reactivity of Nano-B/Al/CuO MIC's." *Combustion and Flame* 156 (2). Elsevier Inc.: 302–9. doi:10.1016/j.combustflame.2008.09.011.

Sullivan, K., and M.R. Zachariah. 2010. “Simultaneous Pressure and Optical Measurements of Nanoaluminum Thermites: Investigating the Reaction Mechanism.” *Journal of Propulsion and Power* 26 (3): 467–72.

Sullivan, K.T., N.W. Piekiel, C. Wu, S. Chowdhury, S.T. Kelly, T.C. Hufnagel, K. Fezzaa, and M.R. Zachariah. 2012. “Reactive Sintering: An Important Component in the Combustion of Nanocomposite Thermites.” *Combustion and Flame* 159 (1): 2–15. doi:10.1016/j.combustflame.2011.07.015.

Sullivan, Kyle T., Wen-An Chiou, Richard Fiore, and Michael R. Zachariah. 2010. “In Situ Microscopy of Rapidly Heated Nano-Al and Nano-Al/WO[sub 3] Thermites.” *Applied Physics Letters* 97 (13): 133104. doi:10.1063/1.3490752.

Tamura, N. 2013. *XMAS: A Versatile Tool for Analyzing Syncrotron X-Ray Microdiffraction Data. Microdiffraction Analysis Local and near Surface Hierarchical Organization of Defects*. *Imperial College Press*. London.

Throop, J.F., J.H. Underwood, and G.S. Legar. 1971. *Residual Stress and Stress Relaxation*. Edited by E. Kula and V. Weiss. Plenum Press.

Trunov, M.A., M. Schooenitz, and E.L. Dreizin. 2006. “Effect of Polymorphic Phase Transformations in the Alumina Layer on Ignition of Aluminum Particles.” *Combustion Theory and Modelling2* 10 (4): 603–23.

Trunov, Mikhaylo a, Swati M Umbrajkar, Mirko Schoenitz, Joseph T Mang, and Edward L Dreizin. 2006. “Oxidation and Melting of Aluminum Nanopowders.” *The Journal of Physical Chemistry. B* 110 (26): 13094–99. doi:10.1021/jp0614188.

Vilms, J., and D. Kerps. 1982. “Simple Stress Formula for Multilayered Thin Films on a Thick Substrate.” *Journal of Applied Physics* 53 (3): 1536–37.

Wang, Haiyang, Guoqiang Jian, Garth C. Egan, and Michael R. Zachariah. 2014. “Assembly and Reactive Properties of Al/CuO Based Nanothermite Microparticles.” *Combustion and Flame* 161 (8). The Combustion Institute.: 2203–8. doi:10.1016/j.combustflame.2014.02.003.

Wang, L.L., Z.A. Munir, and Y.M. Maximov. 1993. “Thermite Reactions: Their Utilization in the Synthesis and Processing of Materials.” *Journal of Materials Science* 28 (14): 3693–3708.

Yeh, C.L., and Y.S. Huang. 2011. “Thermite Reduction of Ta2O5/SiO2 Powder Mixtures for Combustion Synthesis of Ta-Based Silicides.” *J. Alloys Compd.* 509 (21): 6302–6.

Yen, Ng Hsiao, and Lee Yiew Wang. 2012. “Reactive Metals in Explosives.” *Propellants, Explosives, Pyrotechnics* 37 (2): 143–55. doi:10.1002/prep.200900050.

Zheng, B., Y. Lin, Y. Zhou, and E.J. Lavernia. 2009a. “Gas Atomization of Amorphous Aluminum: Part I.Thermal Behavior Calculations.” *Metall. Mater. Trans. B* 40 (5): 768–78.

———. 2009b. “Gas Atomization of Amorphous Aluminum: Part II. Experimental Investigations.” *Metall. Mater. Trans. B* 40: 995–1004.